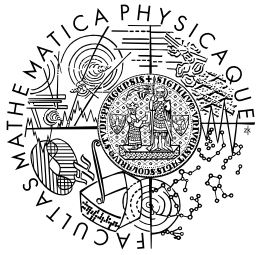

FACULTY
OF MATHEMATICS
AND PHYSICS
Charles University

MASTER THESIS

Bc. Katarína Križanová

Optical and magneto-optical spectroscopy of materials with antiferromagnetic interaction

Institute of Physics of Charles University

Supervisor of the master thesis: RNDr. Jakub Zázvorka, Ph.D.

Study programme: Physics

Study branch: Optics and Optoelectronics

Prague 2020

I declare that I carried out this master thesis independently, and only with the cited sources, literature and other professional sources. It has not been used to obtain another or the same degree.

I understand that my work relates to the rights and obligations under the Act No. 121/2000 Sb., the Copyright Act, as amended, in particular the fact that the Charles University has the right to conclude a license agreement on the use of this work as a school work pursuant to Section 60 subsection 1 of the Copyright Act.

In ..... date ....

Author's signature

Rada by som poďakovala RNDr. Jakubovi Zázvorkovi, Ph.D. a RNDr. Martinovi Veisovi, Ph.D. za ich pomoc pri písaní diplomovej práce a taktiež za ich priateľský prístup ku mne a ostatným študentom na MFF UK.
Za možnosť dokončiť diplomovú prácu vďačím nielen im, ale i mojej rodine a priateľom, ktorým by som sa chcela touto cestou taktiež poďakovať.

Název práce: Optická a magnetooptická spektroskopia materiálov s antiferomagnetickou interakciou

Autor: Bc. Katarína Križanová

Katedra: Fyzikální ústav UK

Vedoucí diplomové práce: RNDr. Jakub Zázvorka, Ph.D., Fyzikální ústav UK

Abstrakt: Jedným z cieľov výskumu v oblasti spintroniky je dosiahnutie účinnej vonkajšej kontroly magnetických momentov. Nekolineárne antiferomagnety v antiperovskitej štruktúre, povedzme Mn_3NiN, vykazujú piezomagnetický jav.
Vďaka tomuto javu nachádzame využiteľnosť spomínaných materiálov. Bez pnutia vykazujú tieto materiály nulový celkový magnetický moment.
Nerovnakosť mriežkovej konštanty medzi tenkou vrstvou a substrátom, na ktorom je nanesený tenký film, vedie ku pnutiu vo vzorke a je možné zaznamenať celkový nenulový magnetický moment.
Spektroskopia magneto-optického Kerrovho javu sa využíva pri štúdiu nekolineárnych magnetických tenkých vrstiev. Štúdium javu pre dva rôzne substráty s vznikajúcim opačným smerom pnutia, ktoré ovplyvní i magnetické usporiadanie antiperovskitov je robené s ohľadom na teplotu vzorky. Výsledky preukazujú porovnateľné spektrálne závislosti s opačným znamienkom Kerrovho javu, čo je spôsobené opačným smerom celkových magnetických momentov.
Elipsometrické merania závisiace od orientácie vzorky sú použité pri štúdiu materiálovej anizotropie a jej zmeny pri magnetickom fázovom prechode pre tenkú vrstvu Mn_3GaN. Spektroskopia optických parametrov a ich vlastná anizotropia je skúmaná pri rôznych teplotách, pod a nad Néelovou teplotou.

Klíčová slova: MOKE antiferomagnet elipsometria spintronika

Title: Optical and magneto-optical spectroscopy of materials with antiferromagnetic interaction

Author: Bc. Katarína Križanová

Department: Institute of Physics of Charles University

Supervisor: RNDr. Jakub Zázvorka, Ph.D., Institute of Physics of Charles University

Abstract: One of the goals of spintronic research is the efficient external control of magnetic moment. Non-collinear antiferromagnets in the antiperovskite structure, such as Mn_3NiN, show a piezomagnetic effect that can be used to utilize these materials in applications. In the strain free state, the material exhibit zero net magnetic moment.
Using strain induced by a lattice constant mismatch between the thin layer and a substrate on which the thin film is applied on a non-zero net magnetic moment can be registered.
Magneto-optical Kerr effect spectroscopy is used to investigate the non-collinear magnetic thin films. The effect of two substrate layers with resulting opposite sign of strain influencing the magnetic ordering of the antiperovskite material is studied with respect to sample temperature. Results show comparable spectral dependence with opposite sign of the Kerr effect caused by the opposite direction of net magnetization moments.
Ellipsometry measurements depending on sample orientation are performed to study the material anisotropy and its change during the magnetic phase transition for the thin film of Mn_3GaN. Spectroscopy of optical parameters and their anisotropy are investigated at different temperatures, below and above the Néel temperature.

Keywords: MOKE antiferromagnet ellipsometry spintronics

Contents

Introduction

Recent progress in antiferromagnetic spintronics introduced new promising concepts of electronic devices, such as ultra-fast computer memories, high density data storage or THz radiation sources.
The detailed overview of the application potential of antiferromagnetic materials can be found for example in the topical review by T. Jungwirth et al. [1]
The authors claim that the Moore's law, the statement that the number of transistors in a dense integrated circuit doubles approximately every two years, might be overcome thanks to the new developments in the field of spintronics. The advances in spintronics are very important as Moore's law is already achieving its limit due to the appearance of quantum effects at small size transistors. [1], [2]
The information technologies coming from the spintronics based on the spin phenomena commonly use ferromagnetic materials. However, there is a new sub-field in spintronics emerging recently which focuses on antiferromagnetic materials. The antiferromagnetic spintronics seems to be very promising due to better properties of antiferromagnetic materials compared to ferromagnets, such as the absence of demagnetization fields, large magneto-transport effects or ultrafast magnetization dynamics. [3]
The beginning of antiferromagnetic spintronics lies in studies on spin transfer and it has reappeared in the last few years with articles reporting the usage of spin-orbit torques to control the magnetic order in the antiferromagnetic materials. [3]
The year 2016 was a breakthrough for antiferromagnets in spintronics. [1] It was the year when the first experimental demonstration of the antiferromagnetic memory device was achieved. Prior to this demonstration, many other studies must have been done and various physical phenomena understood, for example the studies of relativistic charge-spin coupling phenomena (spin Hall effect and spin galvanic effect).
The use of antiferromagnetic spintronics could be beneficial in various technological fields, including THz sources and detectors or magnetic random access memories (MRAMs). These types of memories can operate at higher frequencies while using similar current densities to the ferromagnetic memories. [4], [5]
Apart from information writing, we could also use the new technology for the readout as well. However, several limitations of the readout, such as Ohmic anisotropic magnetoresistance, still remains. In the article by K. Garello et al. [6], the authors claim to demonstrate the fundamental antiferromagnetic memory functionality (electrical writing and readout included) with the expectations of ultra-fast antiferromagnetic memory.
One can distinguish two types of memory devices according to whether the information in it remains (nonvolatile) or not (volatile) after turning off the power source. [7]
Examples of volatile memories are DRAM (Dynamic Random Access Memory) and SRAM (Static RAM). The representant of nonvolatile memory is ROM (Read Only Memory).
Contemporary MRAMs which keep the information in magnetic domains are made of the cells with one tunnel junction and one transistor. [8]
This thesis is devoted to the systematic magneto-optical studies of noncollinear

antiferromagnets in the form of thin films. These materials have either cubic or hexagonal crystal structure. They show piezomagnetic effect and could possibly be used as a memory storage device.
Noncolinear chiral antiferromagnets are interesting due to their interesting magnetic, transport and also structural properties. [9]
Previous studies of noncollinear antiferromagnetic materials discovered their sensitivity to piezomagnetic effects. This was firstly described phenomenologically in 1989. [10] Afterwards, the ab-initio calculations showed the biaxial strain in the material. There are already some electric devices based on magnetostriction, but piezomagnetism observed in thin films of noncollinear antiferomagnets offers many advantages over it.[11] For example, magnetostriction underpinned by spinorbit coupling is quadratic in strain and therefore requires additional external magnetic fields for magnetization reversal, while piezomagnetism is a linear magneto-mechanic coupling. This means that the magnetization can be controlled sensitively with small strains and its direction is switchable by 180°.
Investigated samples of Mn_3NiN in this thesis exhibited a piezomagnetic effect which means that the dependence of the magnetization M on the electric field E is linear, see the figure 1.
This leads us to believe that this type of material could also be possibly used as a memory storage.

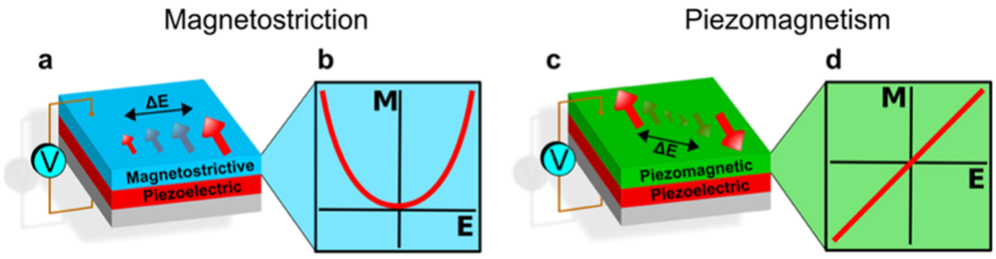

Figure 1: Comparison of magnetostriction and piezomagnetism, from [11]

1. Magnetism

At first, we shall discuss various magnetic structures as the thin layers we have studied were of a magnetic nature. The following information is mainly taken from [12].

1.1 Introduction to magnetism

Magnetic materials have attracted people's curiosity for centuries.
People in Sumer or ancient Greece already knew about the existence of permanent magnets. For example, as written in the article from G. C. Papaefthymiou [13], the ancient Greeks already mined lodestone in the 6^{th} century BC. The oldest written text found talking about the lodestone is from the 7^{th} century BC from Chinese writer Guanzhong. [14]
In modern history, the invention of the horseshoe magnet in 1743 was fairly important as it is the solution to the problem of making a magnet which will not destroy itself after some time because of the demagnetising field.
The apparent resemblance of magnetism and electricity led people to try to find a link between the two. Hans-Christian Oestred finally succeeded. In 1820, he observed that a wire with electric current produces a field which is capable of deviating a compass needle.
The other very important finding for our work was the magneto-optic Farraday effect discovered later in the 19^{th} century. This discovery connected magnetism and light and allowed to study magnetic materials by using the magneto-optical effect. It will be discussed more closely later in this work with other magneto-optic effect, called Kerr effect.
The united theory of magnetism, electricity and light was summarized in now well-known Maxwell's equations (1864).
Magnets, especially electromagnets were widespread already in the end of the 19^{th} century, even though ferromagnetism in solids was not understood at that time. The explanation came after the start of quantum physics and special relativity without which we can not completely understand the mechanism behind it.
One of the reasons the quantum physics is required to be able to explain magnetism is that a classical system in thermal equilibrium cannot have only zero magnetic moment. [15]
The Amperian currents were associated with the intrinsic spin of the electron. As there are just two possible orientations of the spin: up and down. It is spin and orbital interactions which are the source of the electron's intrinsic magnetic moment, so called Bohr magneton μ_B. We can say that the magnetic properties of solids emerge mainly from the magnetic moments of their atomic electrons and the spin-orbit coupling. [12]
Overall, the magnetism arises either from the spin angular moment of the electrons, orbital moments of atoms and change of the orbital moment induced by an external magnetic field or other external force. [15]
We shall discuss the variety of existing magnetic materials.

1.2 Types of Magnetism

The magnetic materials are divided into various classes based on their response to the magnetic field (diamagnetic, paramagnetic,...). [12]
In our work, we studied thin antiferromagnetic layers on diamagnetic substrates.

1.2.1 Diamagnetism

Magnetic atoms are atoms with their spins aligned accordingly. Microscopically, diamagnetism is specific for the substances consisting of not magnetic atoms. Their magnetization which indicates the density of magnetic dipole moments in a material, is induced by the external magnetic field and is usually very weak. [14]
Diamagnetism is a result of a will of material to oppose an applied external magnetic field. This phenomenon emerges from a Lenz-like law, but at the microscopic level [16] of orbital electrons in the material, which acts as if they were closed current loops. We know from Maxwell's equations that if we apply magnetic field, it leads to creation of a current in the loops which acts against the applied external magnetic field. This loops of induced electrical current are called Eddy currents (or also Faucault's currents).
Even though diamagnetism is present in all materials, there can be also other mechanism which can eventually be stronger than diamagnetism itself.
The example of material with diamagnetic properties is copper Cu.

Magnetic susceptibility χ

The magnetic susceptibility is defined as the rate of magnetization of a material as a response to an applied external field. Therefore, it is the ratio of M and H [15]:

$$\chi = \frac{M}{H}, \tag{1.1}$$

where M is magnetization of the material (magnetic moment per one unit of volume) and H stands for applied magnetizing field intensity.
The characteristic feature for the diamagnetic material is a negative value of its magnetic susceptibility χ.
As we mentioned before, diamagnetism is present in all materials even though it is not always predominant. Therefore, diamagnetic susceptibility χ_d is a value that every magnetic material has. χ_d is constant with temperature and its value is material-dependent, however roughly of the order of 10^{-5}. [16]

Langevin diamagnetism

As we mentioned before, according to the Lenz-like law, diamagnetism of the material exhibits itself in the will of electric charges to screen out the external magnetic field. Induced current in atom persists as long as the magnetic field is present.
We usually use the Larmor theorem to describe diamagnetism of atoms. It says that in the presence of a magnetic field, the motion of electrons around the nucleus

is the same as their motion without the presence of the field besides the precession of electrons with angular frequency ω [15]:

$$\omega = \frac{eB}{2m}, \tag{1.2}$$

e, m standing for charge and mass of electron, respectively.
In case that the field is increasing slowly, the movement in rotating system will be the same as before the magnetic field grew. It means that if originally a mean electron current around the nucleon is zero, adding a magnetic field results in appearance of a finite current around the nucleus. This current is equivalent to the magnetic moment pointing to the opposite direction of the external field. Larmor precession of Z electrons is equivalent to electric current [15]:

$$I = (-Ze)(\frac{1}{2\pi}\frac{eB}{2m}). \tag{1.3}$$

First part of the equation in the brackets is the total charge, the second expression in brackets describes the number of circulations per one time unit.
Magnetic moment μ of the current loop is equal to the product of the current intensity and the area of the loop (with radius ρ) $\pi\rho^2$ [15]:

$$\mu = -\frac{Ze^2B}{4m}\langle\rho^2\rangle. \tag{1.4}$$

$\langle\rho^2\rangle = \langle x^2\rangle + \langle y^2\rangle$ is the expected value of the distance squared of an electron from the axes parallel to the field and passing through the nucleus.
Expected value of the square of the distance between an electron and the nucleus is [15] $\langle r^2\rangle = \langle x^2\rangle + \langle y^2\rangle + \langle z^2\rangle$. Therefore, $\langle r^2\rangle = \frac{3}{2}\langle\rho^2\rangle$. Starting from the equation (1.4), we get the diamagnetic susceptibility of the unit volume with N electrons which is the classical Langevin result [15]:

$$\chi = \frac{\mu_0 N\mu}{B} = -\frac{\mu_0 NZe^2}{6m}\langle r^2\rangle. \tag{1.5}$$

The problem is reduced to determining $\langle r^2\rangle$ which can be done by using quantum mechanics.
In dielectric solids, the diamagnetic contribution of ion remains can be described approximately by Langevin theory. However, the contribution of conduction electrons is more difficult to describe.

1.2.2 Paramagnetism

Contrary to the diamagnetic material, paramagnetic material has positive value of its susceptibility χ. The value of χ is generaly small ($\chi = 10^{-6} - 10^{0}$). [7]
The positive value of χ occurs in various cases, for example [15] in atoms with odd number of electrons as the total spin in this case cannot be zero or in free atoms or ions with partially filled inner orbitals.
The positive value of the susceptibility χ indicates that this phenomenon leads to the reinforcement of the external field inside of the material.
It can be explained by unpaired electrons alligning in the direction of the external field. More precisely, the unpaired electrons in paramagnetic materials posses an

arbitrary direction of their magnetic moments. Therefore, if we apply an external magnetic field to a material which is paramagnetic, these uncoupled electrons tend to align in the direction of the applied magnetic field due to their magnetic dipole moment.

Curie law

Using quantum physics, we can obtain the so-called Curie law (for more details see the publication from C. Kittel [15]):

$$\chi \approx \frac{\mu_0 M}{B} = \frac{\mu_0 N J(J+1) g^2 (\mu_B)^2}{3 k_B T} = \frac{C}{T}, \tag{1.6}$$

where N is the total number of magnetic atoms per unit volume, g stands for Landé g-factor, μ_B is Bohr magneton, k_B is Boltzmann's constant, J is the quantum number of angular momentum and C is Curie constant which puts into relation temperature T and magnetic susceptibility of the material.
The general graph for susceptibility of a material following the Curie law is depicted in the picture 1.1.

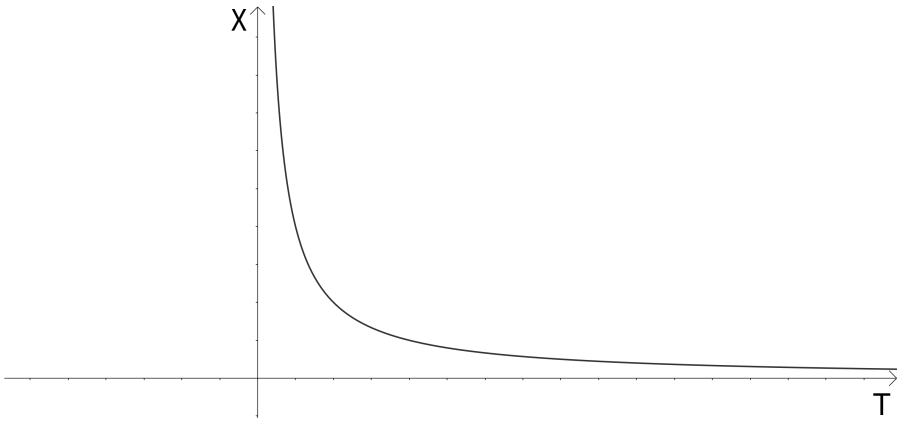

Figure 1.1: Curie law: the dependence of the susceptibility χ on the temperature T follows the equation 1.6

1.2.3 Ferromagnetism

There is a group of materials where microscopic magnetic moments are coupled thanks to an exchange interaction between spins of electrons. This leads to the emergence of spontaneous magnetization (the phenomenon of magnetic ordering at finite temperature and even without any external field). [16]
Ferromagnetism is one of the magnetic ordering types. It can be characterized by a positive exchange parameter (integral).
Both this effect and so called Curie temperature (the critical temperature of a ferromagnet) were explained by Weiss. [12] For that, he used a huge internal molecular field, proportional to the magnetization. Even though this magnetic field does not exist, it seems to be still quite reasonable way how to approximate the inter-atomic Coulomb interaction in quantum mechanics.
Similar to paramagnets, ferromagnets have also unpaired electrons. However, in

a ferromagnetic material, the tendency for the magnetic moments of unpaired electrons to align, parallel to each other (see the picture 1.2), stays even without the application of an external magnetic field. This is due to the spontaneous alignment of the unpaired spins and therefore we observe formation of a spontaneous magnetization of the material. The electron spins and magnetic moments

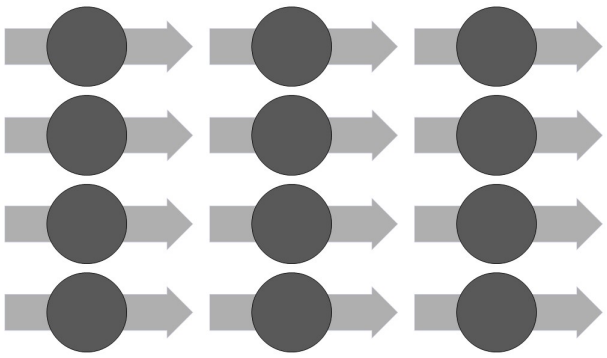

Figure 1.2: Two-dimensional reprezentation: spin lattice of a ferromagnet. The circles represent atoms and arrows are their magnetic moments.

are ordered regularly in a ferromagnet. Therefore, the spontaneous magnetization of a ferromagnet is its characteristic feature. The magnetization of a ferromagnet usually lies along its easy axis. The easy direction is determined namely by the crystal structure of a material or sample shape. [12],[15]

Molecular field theory

As we have already mentioned, the first theory describing ferromagnetism which remains useful to these days was proposed by Pierre Weiss in the beginning of the 20^{th} century.
The theory was coming from the classical paramagnetism of Langevin but was extended to the more complex Brillouin theory of localized magnetic moments.
The basic idea in Weiss's theory is the existence of internal molecular field, proportional to the magnetization of the ferromagnetic material.
The effective field is then:

$$H^i = n_W M + H, \tag{1.7}$$

where n_W is the constant of proportionality, so called Weiss coefficient and H denounces external field.
The Weiss theory foresaw that the state of magnetic saturation is the thermodynamic equilibrium state at all temperatures which are adequately under the Curie point. [17] This is valid as the value of the molecular field is larger than the actual value of internal or external magnetic fields. There is only slight influence of external magnetic fields on the value of the saturation magnetization in the theory.
Nonetheless, seeing that the Weiss molecular field consistently follows the direction of the average magnetization, the magnetization vector is predetermined solely in its magnitude, while its direction is arbitrary. This also explains for

example that a piece of iron can seem to be non-magnetic at room temperature, which is far below the Curie temperature: the magnetization vectors in different parts of the piece of iron only have to negate each other. Overall, there are infinitely many possibilities to reach this type of macroscopically non-magnetic state. In the original Weiss's work, there is a mention of the likelihood that a part of a crystal is magnetized in one direction, and part in the other, opposite direction. The now frequently used term domain structure for the subdivision into uniformly magnetized regions in a crystal was not introduced in the original work but only later, even though Weiss described exactly this phenomenon. [17]

Curie-Weiss law

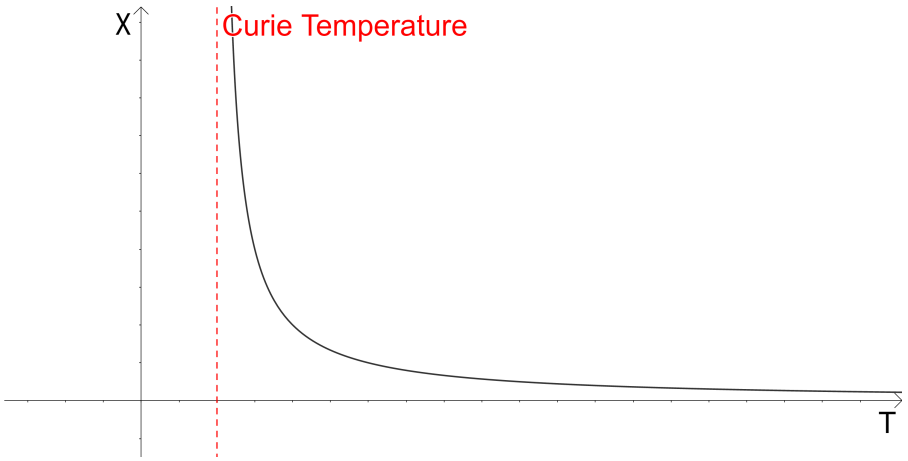

Figure 1.3: Curie-Weiss law for the ferromagnet. The dotted line shows the value of Currie temperature, below which the dependence of susceptibility on temperature is much more complicated.

When we reach the critical temperature of a ferromagnet (Curie temperature) T_C, we observe a reversible collapse of the spontaneous magnetization of the material. That means that for temperatures $T > T_C$, the spontaneus magnetization of the material is zero (paramagnetic state), while for temperatures $T < T_C$, the material comes to the ferromagnetic phase.
For the paramagnetic phase of the material, we can write Curie-Weiss law which describes how the suscepribility χ changes above the Currie temperature [15] (also see the graph in the figure 1.3):

$$\chi = \frac{C}{T - T_C}. \tag{1.8}$$

1.2.4 Energy of a ferromagnet

The variational principle in domain theory says that the vector field of magnetization directions $\mathbf{m(r)}$ is chosen so that the free energy hits its absolute or relative minimum, under one constraint: $m^2 = 1$. [17]
An out-turn of the principle of the minimum energy and of the constant magnetization constraint is that at every point, there is a disappearance of the torque

on the magnetization. The torque conditions are also called micromagnetic equations and are more closely discussed for example in [17].
To begin with domain theory or the micromagnetic equations, we have to consider the magnetization-dependent contributions to the energy.
There are local and non-local magnetic energy terms [17], where the local terms (such as anisotropy energy, the Zeeman energy or the magneto-elastic interaction energy with a stress field of nonmagnetic origin) are based on energy densities given solely by the local values of the magnetization direction.
The non-local magnetic energy terms are the stray field energy and the magnetostrictive self-energy. The second is being associated with interactions of the elastic nature between regions magnetized alongside different axes. The non-local magnetic energy terms are more complicated to be calculated, for more details see the book from A.Hubert et al. [17]
There are two major contributions to the energy of a ferromagnet, that being the atomic-scale electrostatic effect (for example exchange anisotropy or single-ion anisotropy), and magnetostatic effects. The second group implies that we take into consideration also the self-energy of interaction of the material with the field created by itself or the interaction of the material with constant or only slowly changing external magnetic field. [12]
The short-range exchange forces which are behind ferromagnetism are stronger than the magnetostatic interactions. Nevertheless, the magnetostatic interactions still play an important role in ferromagnets as the domain structure and magnetization process are determined by them. [12] Dipole-dipole interactions vary as r^{-3}. Thanks to their long-range nature, the weak interactions control the magnetic microstructure. Demagnetization fields are similar in magnitude, even though slightly smaller, as the magnetization of a ferromagnetic material.
As the magnetic part of the Lorentz force is without exception perpendicular to the motion, the magnetic fields do not work on electric currents or charges in motion. It is not possible to relate a potential energy function to the magnetic force. Thus, we have to consider also the work done by the transient electric fields when setting up a specific magnetic configuration, to be able to calculate the associated energy. [12]
According to the variational principle derived from thermodynamic principles, the vector field of magnetization directions [17]

$$m(r) = \frac{J(r)}{J_s} \tag{1.9}$$

is decided so that the overall free energy comes to either absolute or relative minimum. [17] We do not take into account the very rare cases when the constraint $m^2 = 1$ is not valid because of the changing of the saturation magnetization J_s in a micro-magnetic configuration.

Exchange energy

When we talk about the exchange energy of a ferromagnet, we distinguish between volume exchange stiffness energy and exchange interface coupling. [17]
The first one is associated with the core property of a ferromagnet, that being its prioritizing of a constant equilibrium magnetization direction. Any deviation from this state of equilibrium gives rise to an energy penalty. This can be

characterized by the following "stiffness" expression [17]:

$$E_x = A \int \nabla(m)^2 \, dV, \tag{1.10}$$

where A stands for a material constant (exchange stiffness constant) which is generally dependent on temperature. Its value for zero temperature is related to the Curie temperature T_C [17]:

$$A(0) \approx \frac{k_B T_C}{a_L}, \tag{1.11}$$

a_L is a lattice constant and k_B stands for Boltzmann's constant.
Exchange interaction coupling occurs at interface of two ferromagnets. From phenomenological approach, this can be illustrated by the surface energy density expression [17]:

$$e_{coupling} = C_{bl}(1 - m_1 \cdot m_2) + C_{bq}(1 - (m_1 \cdot m_2)^2), \tag{1.12}$$

where m_1 and m_2 stand for the magnetization vectors at the interface of two ferromagnets, C_{bl} and C_{bq} are the bilinear and biquadratic coupling constants, respectively.
In the case that the bilinear coupling constant is positive, the parallel orientation of the magnetization in both media is preferred, we talk about ferromagnetic coupling. On the contrary, if the constant has a negative value, an antiparallel alignment is favoured (antiferromagnetic coupling).
A 90° relative orientation is possible in case a value of the biquadratic coupling constant is negative.

Anisotropy energy

The energy of a ferromagnet is, as a result of spin-orbit interactions, dependent on the direction of the magnetization in relation to the structural axes of the ferromagnet. This is described by anisotropy energy. [17]
There are crystal anisotropies of the undisturbed crystal structure and induced anisotropies which account deviations from ideal symmetry (lattice defect,etc.).
Note that shape effects are not being described by the anisotropy but they are one of the factors taken into account in stray field energy.
It does not matter where the origin of anisotropies is from, they have to follow the symmetry of the system at all cases. That is the reason why expansions in terms of spherical harmonics are applied to describe the majority of contributions. The higher-order contributions are usually not taken into account as the thermal agitation of the spins usually averages it out.

Zeeman energy

The external field energy, also called Zeeman energy, describes the interaction energy of the vector of magnetization with an external field H_{ex}. The expression for Zeeman energy is [17]

$$E_{Zeeman} = -J_s \int H_{ex} \cdot m \, dV. \tag{1.13}$$

J_s is already mentioned saturation magnetization.
In case we have a uniform H_{ex}, the Zeeman energy is determined solely by the average magnetization and does not depend on the particular domain structure of the magnetic material.

1.2.5 The hysteresis loop and magnetic domains

The hysteresis loop

If we consider a material under an applied magnetic field **H**, we know that this results also in the appearance of Zeeman energy which is described in previous subchapter. This results in the so-called magnetization process (or magnetization reversal) [16] which is the tendency of the magnetization to align parallel to the applied external field **H**.
The process is registered by moment or magnetization measurements done for example by magnetometers or magnetic microscopes, respecively. The results of these measurements are often registered in hysteresis loop (also called magnetization curve or loop), see the picture 1.4.

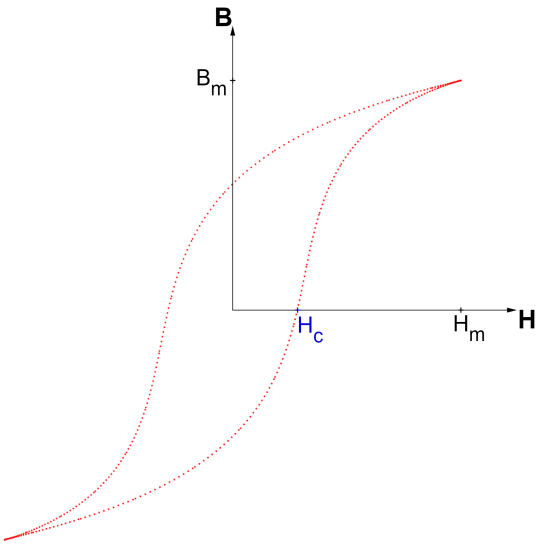

Figure 1.4: Typical hysteresis loop: the dependence of **B** on **H**. B_m and H_m are the maxima of attainable values of **B** and **H**. H_c stands for coercivity.

The coercive field depicted in the picture 1.4 is the field opposing an applied magnetic field. Its value is determined by the intersection with x axis which is the point when the average magnetization projected to the direction of the field disappears.

Domains and domain walls

The hysteresis loop shows us the magnetic characterization on a macroscopic level, while some details of magnetization at the microscopic level might stay hidden. [16] Therefore, we must remember that the hysteresis loop does not give us the full characteristics of magnetization reversal.
Pierre Weiss postulated the occurrence of magnetic domains in his mean field

theory. They are regions where every region has to a great degree uniform magnetization and its direction may vary from one domain to another.
Probably the first evidence of the existence of magnetic domains and observing the attraction of nanoparticles by the locus of domain walls was done in 1931.
One year after that, Felix Bloch analytically described the change of magnetization between two different domains, also called domain wall.
The basic principles of the energetic study of magnetic domains were suggested by Landau and Lifshitz.
There are two effects causing the formation of magnetic domains, which mostly take place at the same time. The first one is energetics, the creation of domain walls is compensated by the reduction of dipolar energy which would be that of a remaining uniformly magnetized body. The second reason of magnetic domain creation is the magnetic history which is connected with the hysteresis loop.

1.2.6 Ferrimagnetism

Sublaticces and chain of magnetic moments

Negative exchange interaction is an indicator of magnetic ordering determined by lattice topology. There are structures which contain more than one magnetic sublattice, for example ferrimagnet or even antiferromagnet [12] which is the material we used also in our measurements.
In the case that the sublattice magnetizations do not compensate each other, a nontrivial net spontaneous magnetization is registered.
Nowadays, it is possible to measure the sublattice magnetization thanks to neutron scattering.
Individual magnetic chains do not have magnetical ordering, for example, because of the energy cost to reverse a block of spins.
The model of ferromagneism is based on chain of atoms.
In case of multiple chains and considerable interchain interactions, the interchain coupling is able to cause magnetic ordering. For further information see [12]. The magnetic order with long distance range is non existent. However, the magnetic excitation may still occur.

Ferrimagnetism

We say that a material is ferrimagnetic if the magnetization of the two sublattices is not the same in overall magnitude and if these do not compensate each other. This is depicted in the figure 1.5 showing a spin lattice of a ferrimagnet.
Ferrimagnetism is a magnetic ordering resulting from negative exchange coupling occurring between moments of different sizes. The ordering temperature of a ferrimagnet is called Curie temperature. [16] It may occur that each sublattice of a ferrimagnet is ordered under different temperature.
The mentioned spontaneous magnetization occurs below the Curie point, while no magnetic order is registered above it. It means that it becomes paramagnetic above Curie temperature. Nevertheless, there can also be another important temperature in a ferrimagnet, so called compensation temperature.
The compensation temperature can be found in some ferrimagnetic materials under the Curie point. The opposing moments tend to compensate at this tem-

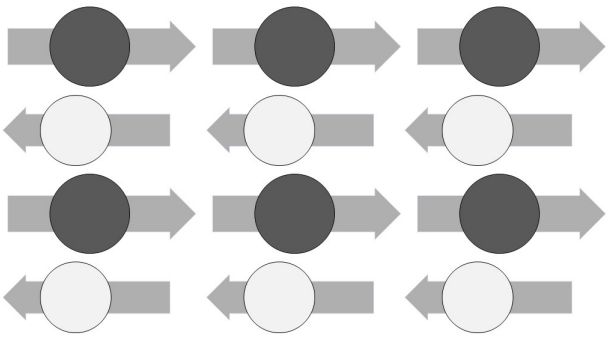

Figure 1.5: Two-dimensional model: spin lattice of a ferrimagnet, chains with different direction and amplitude of magnetization. The net magnetization is not zero.

perature so that overall, net magnetization becomes zero. [12] This is because of the different temperature dependence of each sublattice which compensate each other at one point (the compensation temperature).

1.2.7 Antiferromagnetism

The magnetic material which is of the most importance for this work is very similar to previously mentioned ferrimagnet. It is an antiferromagnet. This magnetic ordering has been known since the 1930s. [18]
Antiferromagnetism is a magnetic ordering which is also a product of a negative exchange energy but with antiparallel alignement of neighbouring spins which overall sum up to a zero net magnetization. [16]
The ordering of the magnetic moments of the atoms in an antiferromagnet ordering align regularly. The neighbours have the opposite direction, see the picture 1.6 depicting the spin lattice of an antiferromagnet. That is why we can talk about several equal sublattices in case of an antiferromagnetic material.

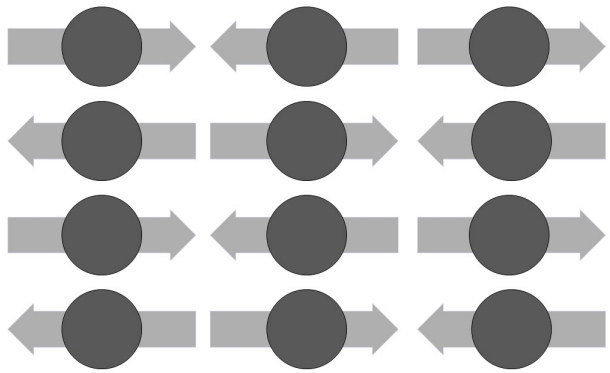

Figure 1.6: Two-dimensional model: spin lattice of an antiferromagnet. Circles depict the atoms which might be of different elements, arrows depict their spins. The net magnetization of antiferromagnet sums up to zero.

In the case of antiferromagnetic material, a crystal lattice is divided into two or more atomic sublattices in one plane which are ordered in a way that the total magnetization is zero.
The typical feature for so called Néel point (the antiferromagnetic ordering transition) is a small peak in the magnetic susceptibility, see the figure 1.7. [12]
Susceptibility χ increases with increasing temperature until the mentioned Néel temperature. After that, the material becomes paramagnetic.
For this paramagnetic state, the Curie-Weiss law (equation 1.8) transforms to the following form [7]:

$$\chi = \frac{C}{T + T_N}, \tag{1.14}$$

where T_N is Néel temperature.

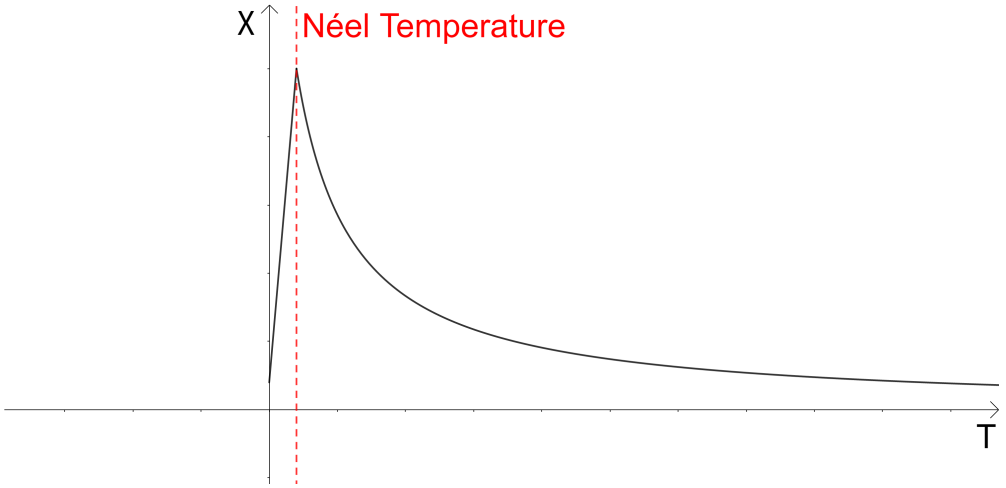

Figure 1.7: The evolution of susceptibility for an antiferromagnet. Below the Néel temperature, the material is antiferromagnetic, above it becomes paramagnetic. A small peak at Néel point helps to identify it.

2. Magneto-optics

2.1 Light and polarization of light

In magneto-optical spectroscopy, we study materials and their magneto-optical properties. For that, polarized light is used, therefore the brief introduction to this topic is needed for further understanding.
The propagation of light is a special case of electromagnetic waves which are visible to human eyes. It can be described by the wave equation, derived from well-known Maxwell's equations:

$$Rot\vec{E} + \frac{\partial \vec{B}}{\partial t} = 0 \tag{2.1}$$

$$Rot\vec{H} - \frac{\partial \vec{D}}{\partial t} = \vec{j} \tag{2.2}$$

$$Div\vec{D} = \rho \tag{2.3}$$

$$Div\vec{B} = 0. \tag{2.4}$$

$\vec{E}$, $\vec{D}$, $\vec{B}$ and $\vec{H}$ stand for electric field vector, electric displacement vector, magnetic induction and magnetic field, respectively. $\vec{j}$ denounces electric current density and ρ stands for free electron charge density.
Using the above mentioned Maxwell's equations and material equations for $\vec{B}$, $\vec{D}$ and $\vec{j}$, we can get the wave equation for homogeneous isotropic dielectric medium:

$$\vec{E} - \mu\epsilon\frac{\partial^2 \vec{E}}{\partial t^2} = 0, \tag{2.5}$$

μ and ϵ stand for permeability and permittivity of the medium. One of the solutions of the equation 2.5 is a harmonic monochromatic wave (in case that the wave propagates in the direction of axis z) [19]:

$$\vec{E}(z,t) = \vec{e_x}E_x(z,t) + \vec{e_y}E_y(z,t). \tag{2.6}$$

By simple modifications, we can get to the equation of ellipse for the components of $\vec{E}$. The light is generally polarized elliptically but it might get to special cases of circular polarization or even linear polarization. Depending whether the vector $\vec{E}$ rotates clockwise or counterclockwise (when we look against the direction of propagation of the light), we talk about right-hand or left-hand elliptical polarization, respectively.
The polarization of a plane monochromatic wave can be described in Jones formalism by using Jones vectors. For deriving the Jones vectors, we use complex representation of $\vec{E}$. For more details see for example the publiction from P. Maly [19].
The Jones vectors of linear and circular polarization of the light are in the table 2.1. The optical components such as polarizers or compensators which change the polarization of the light are represented by the Jones matrices.

Polarization of light	Jones vector
Linear, axis x direction	$\begin{pmatrix}1\\0\end{pmatrix}$
Linear, axis y direction	$\begin{pmatrix}0\\1\end{pmatrix}$
Linear, angle α from axis x	$\begin{pmatrix}\cos\alpha\\\sin\alpha\end{pmatrix}$
Circular, left-handed (+) and right-handed (-)	$\frac{1}{\sqrt{2}}\begin{pmatrix}1\\\pm i\end{pmatrix}$

Table 2.1: Jones vectors of various types of light polarization, for further information see the publication from P. Maly [19]

2.2 Magneto-optic effects

In general, magneto-optical effects are based on phenomena arising when the interaction between light and matter, usually subjected to an external magnetic field, occur. This can be done even without application of any external magnetic field in the case of magnetically ordered matter such as ferromagnets, ferrimagnets or antiferromagnets. [20]
These effects are based on the breakage of isotropy of the environment because of the magnetic field which leads to the change of transmitted or reflected light from this type of material for s and p polarizations, respectively. [21]
Both Faraday and Kerr effect mentioned in this section are related to electron spin-orbit coupling. [12] These methods indirectly permit us to collect information about the magnetization state of a material. [16]
Overall, we can say that magneto-optical effects occur as a response to a magnetic field. In this work, we consider only linear contribution.

2.2.1 Faraday effect

All magneto-optics started probably in 1845 with Michael Faraday's discovery. Faraday found the connection between light and magnetism [22] when he discovered that a block of glass subjected to a magnetic field is optically active (responds to the electromagnetic field by rotation of the plane-polarized light). He came to that conclusion by observing the rotation of plane-polarized light in the direction of propagation after transmission through the glass. Faraday originally used a paramagnetic glass. However, this effect is present as well when the light traverses a diamagnet or a transparent, spontaneously magnetized ferrimagnet or ferromagnet.
This mentioned angle of rotation of the plane of polarization Θ_F is proportional to the optical path length:

$$\Theta_F = V \int \mu_0 \mathbf{M}\, dl, \tag{2.7}$$

where V is the so-called Verdet constant of the material, μ_0 permeability and $\mathbf{M}$ induced magnetization of the material.
In the simplest possible case, where the sample is uniformly magnetized, the rotation of the polarized light is proportional to the magnitude of magnetic field applied H and distance the light travelled through the glass L:

$$\Theta_F = VHL. \tag{2.8}$$

The Faraday effect can be explained from a phenomenological point of view as the difference of the refractive indexes for the left-handed and right-handed circularly polarized light when the material is in a magnetic field.
The sense of rotation may be reversed by switching the direction of the magnetization of the material. [12], [20]
One of possible applications for the Faraday effect is Faraday rotator. It is an apparatus which can detect optical bistability. It consists of phase-matching films, a coil made of semi-hard magnetic material, a polarizer and a polarization splitter and finally semi-cylindrical lenses.
The plane of linearly polarized light entering to the Faraday rotator is rotated due to a magnetic field applied parallel to the direction of light propagation. [20]
The rotation follows the equation 2.8.

2.3 Magneto-optical Kerr effect (MOKE)

2.3.1 MOKE and its various configurations

At the end of the 19^{th} century, John Kerr discovered [23] that there was a shift (less than 1°) of the plane of polarization of the light reflected by a ferromagnetic mirror (the polished iron pole face of an electromagnet) in case the mirror is magnetized perpendicularly to its surface. The direction of the shift switched with magnetization being reversed. [12],[24]
Phenomenon arising from the reflection from the surface is a method used to study thin layers of a material. Its limit is solely in the depth of the penetration of the light and optical cleanness of the studied material, otherwise there are no specific criteria for the sample.
We know several configurations of MOKE (see the figure 2.1), that being:

- **Polar**: the sample is magnetized perpendicularly to the surface
- **Longitudinal**: the magnetization vector lies in the plane of incidence (which is the plane of the sample)
- **Transverse**: the magnetization is perpendicular to the plane of incidence of the light (but lies in the sample plane)

In the case of polar and longitudinal MOKE, the influence of the magnetization is registered only as a change of an angle and ellipticity of originally linearly polarized light after the reflection from a magnetic material.
Kerr rotation Θ_K and ellipticity e_K of polar and longitudinal MOKE are:

$$\Theta_K = \Psi_K \cos \Phi_K \tag{2.9}$$

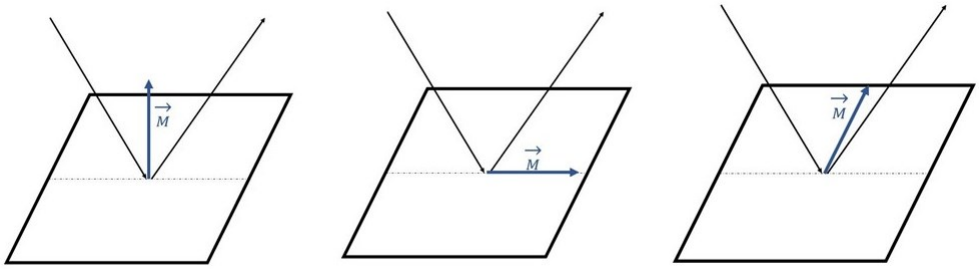

Figure 2.1: Three basic configurations of magneto-optical Kerr effect: polar, longitudinal and transverse (from left to right)

and

$$e_K = \Psi_K \sin \Phi_K, \tag{2.10}$$

where

$$\Psi_K = |\frac{\mathbf{K}}{\mathbf{r}}|,$$

K being the propagation vector, and Φ_K is the phase difference between K and r. The magnitude of the Kerr effect is generally small. For example, the polar Kerr angles for normal incidence are usually only 0,01° or less for materials such as iron, cobalt or nickel. [20]
Often, MOKE might be used as a domain imaging technique in Kerr microscope. Also, we can use Kerr or Faraday effect for investigation of magnetization processes. It is possible if the beam of light is a lot bigger than the domain area so that the domains do not average out. Then, we register the net magnetization. [12]
Magneto-optical spectroscopy overall represents powerful non-destructive method to measure properties of magnetic materials and various nanostructures.
For our measurements, we used the method of rotating analyzer in longitudinal MOKE and also tried the polar MOKE configuration.

Gyrotropic permittivity

In some cases, the permittivity tensor gives us the full description of the interaction occurring between light and material. [25]
In a magnetic field and in magnetic materials, there is a violation of a stability between the total contributions of the clockwise and counterclockwise processes to the permittivity. This leads to a rotation of the plane of polarization of light or eventually to a difference between the absorption coefficients of the light with different polarizations. This phenomenon is strongly dependent from the material, more precisely, it depends on its electron energy spectrum. [20] Thanks to the wave equation 2.5, some components of the tensor are not independent [25]:

$$\epsilon = \begin{pmatrix} \epsilon_{11} & \epsilon_{12} & \epsilon_{13} \\ -\epsilon_{12} & \epsilon_{22} & \epsilon_{23} \\ -\epsilon_{13} & -\epsilon_{23} & \epsilon_{33} \end{pmatrix}. \tag{2.11}$$

As we have already said before, we consider only effects linear in magnetization which means that the diagonal elements are approximately identical.
Taking into account the configuration of the MOKE measurements, the expression for the permittivity tensor gets even easier as some components vanish. For Polar MOKE, we get [25]:

$$\epsilon = \begin{pmatrix} \epsilon_1 & \epsilon_2 & 0 \\ -\epsilon_2 & \epsilon_1 & 0 \\ 0 & 0 & \epsilon_1 \end{pmatrix}, \tag{2.12}$$

where off-diagonal elements of permittivity tensor are proportional to magnetization of the material.
It is also possible to divide the tensor to symetric and antisymetric part [20]:

$$\epsilon = \begin{pmatrix} \epsilon_1 & 0 & 0 \\ 0 & \epsilon_1 & 0 \\ 0 & 0 & \epsilon_1 \end{pmatrix} + \begin{pmatrix} 0 & ig & 0 \\ -ig & 0 & 0 \\ 0 & 0 & 0 \end{pmatrix}, \tag{2.13}$$

and $\mathbf{D}$ can be rewritten as follows [20]:

$$\mathbf{D} = \epsilon_0 \mathbf{E} + i(g\vec{E}) + b(\mathbf{E} - m(m \cdot \mathbf{E}). \tag{2.14}$$

The element g is gyration vector. The gyrotropic effects of a material can be described by the second part of the equation 2.13.

2.4 Method of the rotating analyzer and Jones formalism

The method used in our measurement is that of rotating analyzer. We put our sample in a cryostation with electromagnet creating magnetic field aligned along one axes, slightly under 1 Tesla.
The apparatus assembly, depicted in the picture 2.2, consisted of:

1. Source of light
2. Collimating lens
3. Polarizer
4. Beam splitter, lens, chopper, detector
5. Cryostation with the sample
6. Iris diaphragm
7. Rotating analyzer
8. Detector

We studied magneto-optical Kerr effect by detecting the reflection of the light from a surface of a thin film on substrate.
The measurement setup presented in the picture 2.2 shows the method with nearly crossed polarizers. We assume normal incidence of light, the Kerr effect

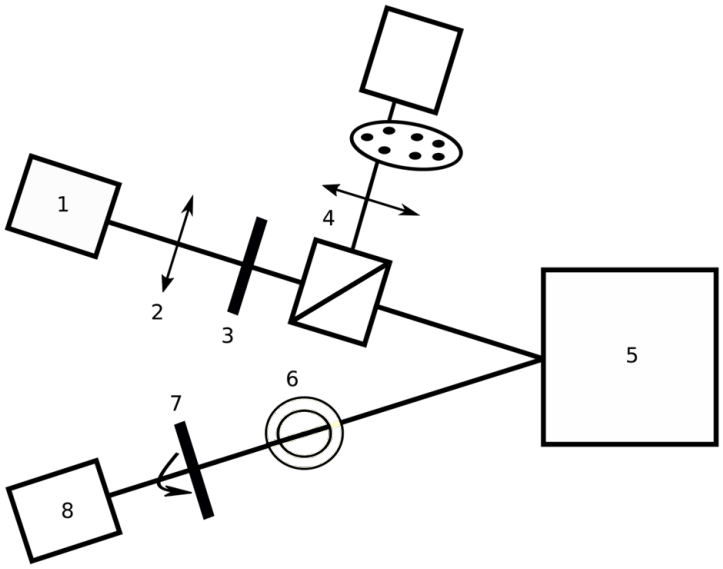

Figure 2.2: Schematic picture of the mesurement setup based on the method of rotating analyzer.

can be represented by magneto-optical angle Θ_K.
The light entering the experiment is not polarized, we put a polarizer in its way and we get a light that is linearly polarized. The p-polarization of light chosen by us is reflected from the sample placed in cryostation with a magnetic field of known value (the order of magnitude of 100 mT).
Light impacts the second polarizer (rotating analyzer), rotated by an angle α from the first polarizer. The intensity of light is detected by a CCD spectrometer.
It is possible to derive the dependence of a light intensity with respect to the angle α. For that we use the Jones formalism.
We multiply the Jones matrices of the components used in our measurement, we assume there were no other components apart from the polarizers and the sample changing the polarization of the light (we neglect the window of the cryostation due to the normal incidence). We start with the polarization state right after the transmission through the first polarizer. We get:

$$M = \begin{pmatrix} \sin^2\alpha & \sin\alpha\cos\alpha \\ \sin\alpha\cos\alpha & \cos^2\alpha \end{pmatrix} \begin{pmatrix} 1 & -\Theta_K \\ -\Theta_K & -1 \end{pmatrix} \tag{2.15}$$

As we mentioned before, we chose p-polarization. This polarization is represented by the following Jones vector $\begin{pmatrix} 0 \\ 1 \end{pmatrix}$.
Jones vector of the detected light is then:

$$J = \begin{pmatrix} -\Theta_K - \sin\alpha\cos\alpha \\ -\Theta_K \sin\alpha\cos\alpha - \cos^2\alpha \end{pmatrix} \tag{2.16}$$

Knowing that the intensity of light detected by a CCD spectrometer is [25]

$$I = \frac{1}{2} J^+ J \tag{2.17}$$

and using (2.16), we get the dependence of intensity I on Kerr magneto-optical angle Θ_K:

$$I = \frac{1}{2}\Theta_K \sin 2\alpha + \cos^2 \alpha + \Theta_K^2 \sin^2 \alpha \tag{2.18}$$

As Kerr effect is very small, we can neglect the orders of Θ_K higher than Θ_K which leads us to an approximate dependence of intensity:

$$I \approx \Theta_K \sin 2\alpha + \cos^2 \alpha + C \tag{2.19}$$

where C is a constant corresponding to a dark current in CCD or other constant effects.
As we do not consider misalignment of polarizers, we measured Kerr effect for both magnetic field directions, we made a difference of the two polarities of Kerr magneto-optical angle of and then divided the value by two. We could do this as the linear magneto-optical effects are odd in magnetization while the misalignment does not have such symmetry in magnetization. [25]

2.5 Ellipsometry

Ellipsometry is an optical measurement technique usually used to determine the thickness, refractive index or absorption of a thin layers or a layer on a substrate by fitting the measured optical constants. This all is possible even for a bulk material .
Eventually, the ellipsometry can be used as a complementary method to MOKE measurements in a way that ellipsometry determines the diagonal part of the permittivity tensor. MOKE has information about the off-diagonal part. Using both methods, one can calculate the whole permittivity tensor of a material or sample. Measuring the spatial asymmetry (or symmetry) of the sample at various temperatures can help us to determine the eventual phase transition of a magnetic material represented by change in optical parameters - change of reflectivity for example.

2.5.1 Law of reflection and Snell's law

In ellipsometry, we study the change in the refracted polarized light from the interface, see the picture 2.3.
The law of reflection tells us that the angle of incidence and angle of refraction are the same:

$$\Phi_i = \Phi_r, \tag{2.20}$$

while the law of refraction, also called Snell's law tells us what happens with transmitted light:

$$n_1 \sin \Phi_i = n_2 \sin \Phi_t. \tag{2.21}$$

2.5.2 Amplitude ratio Ψ and phase difference Δ

Two values are measured in ellipsometry, that being an amplitude ratio Ψ and phase difference Δ. These are the amplitude ratio and phase difference of the two polarizations of the light s (senkrecht=perpendicular) and p (parallel), also called

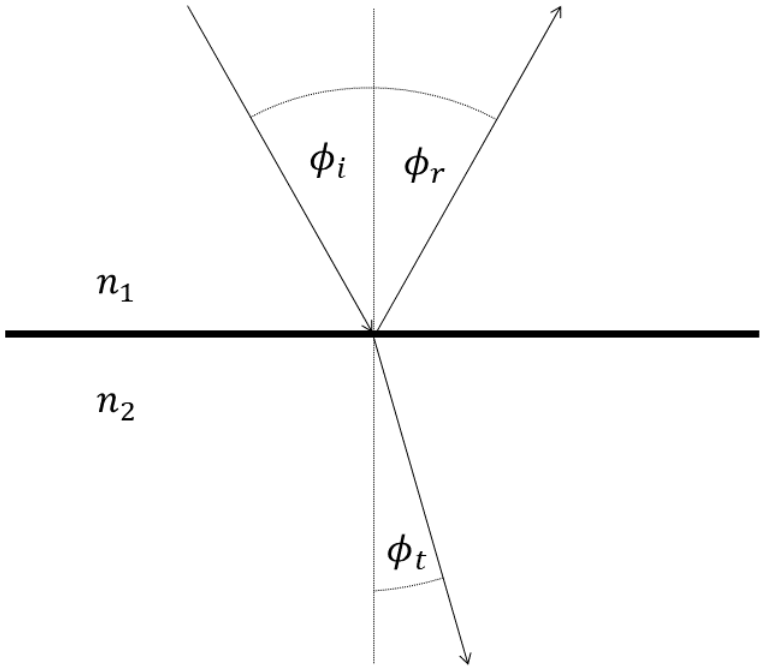

Figure 2.3: Refraction and transmission at the surface of a medium with different index of refraction

transverse-electric (TE) and transverse-magnetic (TM). [26] These two measured quantities are always correct, however, the other calculated values, such as thickness of the material or refractive index are dependent on the model based on which we calculate them and might not be always subjected to the quality of the fit. [27]
To be able to determine them, we use Fresnel reflection coefficients which are calculated by dividing the amplitude of reflected by incoming light of one polarization (s or p). [19], [27]
The equation for coefficient of reflection for p-polarization is [27]:

$$r^p = \frac{\tilde{N}_2 \cos\Phi_1 - \tilde{N}_1 \cos\Phi_2}{\tilde{N}_2 \cos\Phi_1 + \tilde{N}_1 \cos\Phi_2}. \tag{2.22}$$

Similarly, for s-polarization we get:

$$r^s = \frac{\tilde{N}_1 \cos\Phi_1 - \tilde{N}_2 \cos\Phi_2}{\tilde{N}_1 \cos\Phi_1 + \tilde{N}_2 \cos\Phi_2}. \tag{2.23}$$

We replaced refractive index n with complex refractive index N.
It is possible to express the reflectance thanks to the Fresnel reflection coefficients. Reflectance is the ratio of outgoing and incoming intensity of the light. It is:

$$\Re^p = \mid r^p \mid^2 \tag{2.24}$$

for p-polarization and accordingly for s-polarization.
If we include also the phase difference Δ coming from the reflection from the sample, where δ_1 and δ_2 are phase differences before and after the reflection of the light:

$$\Delta = \delta_1 - \delta_2. \tag{2.25}$$

Then, the amplitude ratio Ψ can be calculated as follows [27]:

$$\tan \Psi = \frac{\mid R^p \mid}{\mid R^s \mid} \tag{2.26}$$

and phase difference Δ is determined as

$$\tan \Psi \exp i\Delta = \frac{R^p}{R^s}. \tag{2.27}$$

3. Crystal structure of magnetic materials

3.1 Crystal structure of solids

To describe the ordered positioning of atoms, molecules or ions of crystalline material, we use the crystal structure of solids.
The unit cell is the smallest periodical unit in the crystal material and at the same time contains the full symmetry of the corresponding crystal structure. The symmetry and structure of the crystal is made of repetitive unit cell translation along its principal axes, see the picture 3.1. These translation vectors determine the nodes of the Bravais lattice.

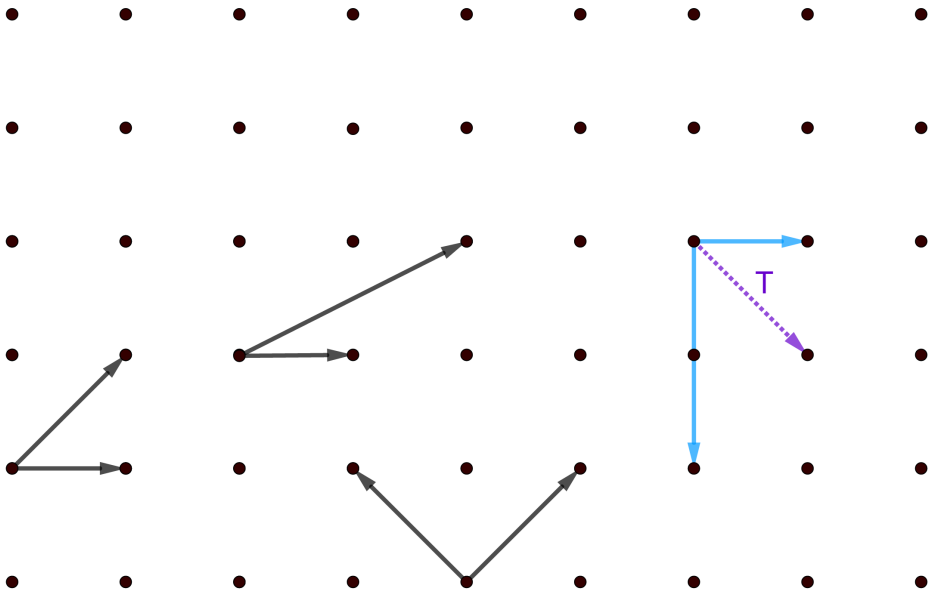

Figure 3.1: Lattice points in two dimensions are depicted with black points. The pair of vectors of black color are the possible unit cell vectors while the blue ones are not as we cannot make a lattice translation T out of its multiplication by integer number.

In two dimensions, the point groups correspond to five different types of lattices. In three dimensions, the variety is bigger, we have overall fourteen types of crystal lattices.
These can be regrouped into seven unit cells, that being: triclinic, monoclinic, orthorombic, tatragonal, cubic and hexagonal. [15]
The crystal structure of the materials used in our measurements was cubic as determined by XRD diffraction in the article from D. Boldrin [11]. Therefore, we shall discuss this type of confinement more closely.

3.2 Cubic crystal structure

We know three types of cubic cells:

1. simple cubic (sc)
2. body-centered cubic (bcc)
3. face-centered cubic (fcc)

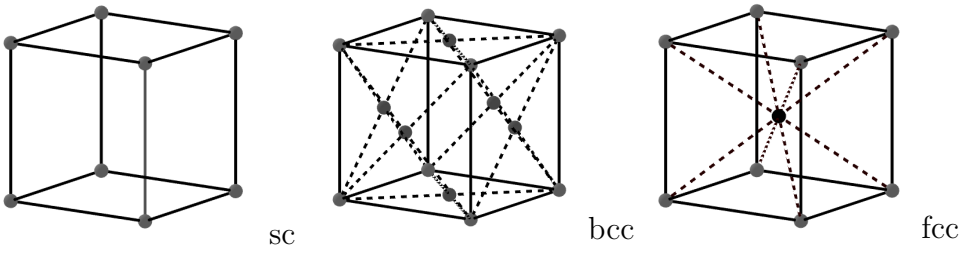

Figure 3.2: Three types of cubic cells

Simple cubic crystal system holds one lattice point at each corner of the cube, this point is shared in between all the neighbouring cubes. Therefore, one simple cube contains overall one lattice point per unit cell ($\frac{1}{8} \cdot 8$). The simple cubic crystal structure can be for example found in polonium (Po).
The body-centered cubic system has as well one lattice point at each corner of the cube shared in between the eight neighbouring cubes as it was in sc. Additionally, we have a half contribution from each point in the middle of each face of the cube as it is shared between two cubes, bcc has in total four lattice points per unit cell ($\frac{1}{8} \cdot 8 + \frac{1}{2} \cdot 6$).
The bcc structure can be for example found in iron (Fe).
The face-centered cubic system has additionally to sc cube one point in the middle of the cube that is not shared, fcc has overall two lattice points per unit cell ($\frac{1}{8} \cdot 8 + 1$).
A well known compound which has fcc structure is sodium chloride (NaCl).

3.3 Antiferromagnets with cubic structure

A special section of solid-state physics, applicable also in antiferromagnets, is a study of material's magnetic structure. It corresponds to ordering of spins, typically accordingly to the materials' crystallographic lattice structure.
The magnetic structure of the material can be determined for example thanks to neutron diffraction. [15]
Accordingly to the magnetic structure of the material, its net magnetization can be determined.
As written in [12], a feature of various number of crystal lattices is that there is a freedom in choice of several different ways how to obtain the two equal antiferromagnetic sublattices. Different spin configurations have also different topology. The orientation of the spins relative to the crystal axes is an issue determined separately by magnetocrystalline anisotropy.

Overall, there are four possibilities of antiferromagnetic modes configuration in a simple cubic lattice structure. For completely decoupled body-centered cubic antiferromagnetic structures there exist two types and for the face-centered cubic structure we know four types of magnetic modes but one of them is ferromagnetic. This means that there might be several configurations for one antiferromagnetic material.
Various configurations for antiferromagnet with simple cubic lattice are depicted in the picture. The configuration of the material depends on its easy axes.

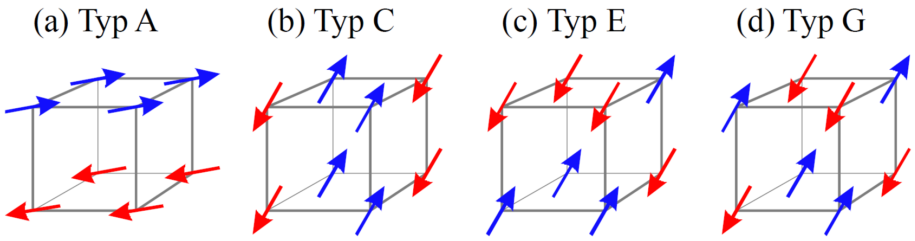

Figure 3.3: Various configurations of an antiferromagnet with simple cubic structure, taken from [28].

Our antiferromagnetic samples with body-centered cubic structure had also more than one possible configurations.

3.4 Noncolinear antiferromagnets

Néel temperature

As we mentioned before, the antiferromagnets possess two (in the least complicated case) magnetic sublattices A and B, which are antiparallely ordered:

$$\boldsymbol{M_A} = -\boldsymbol{M_B}. \tag{3.1}$$

The net magnetization of the material

$$\boldsymbol{M} = \boldsymbol{M_A} + \boldsymbol{M_B}$$

is zero if the contribution from external field **H** is also zero. [12]
If the temperature of the material is at the Néel point, the magnetization of each sublattice falls to zero and spontaneous magnetization of the sublattices can be expressed by the Brillouin function, for more details see the book from J. Coey [12]. The susceptibility of the antiferromagnet is at its maximum. [15]
When the temperature of the material is *higher than* T_N, the material is in the paramagnetic state and the susceptibility obeys Curie-Weiss law. The easiest case of an antiferromagnet is probably the one with two magnetic sublattices with opposite directions of magnetization. In this case, the axis along which are the two sublattice magnetizations is chosen by magnetocrystalline anisotropy, it becomes an easy axes.
In the samples we used in our measurements, the magnetization lies along the (111) axes.
The magnetic response of antiferromagnet *below the Néel point* is determined

from the proportion of **H** and direction of the antiferromagnetic easy axis.
The absence of the shape anisotropy comes from the fact that demagnetizing field of an antiferromagnet is zero when **M**=0. Nonetheless, the antiferromagnetic domains may still be formed due to entropy at finite temperatures. [12]

3.4.1 Collinear and Noncollinear antiferromagnets

The antiferromagnets with the simplest magnetic structure are collinear. They are composed of several pairs (or one pair) of magnetic sublattices of identical magnetic ions which are in the same crystallographic positions. [29] The sublattices have reverse orientation of the magnetization to each other.
A more complicated configuration is that of noncollinear antiferromagnet with a tilting angle between the magnetizations of the sublattices. Therefore, the atomic magnetic moment directions are not parallel to each other, we talk about canted antiferromagnetism. [7], [29]
Note that even in the case of canted antiferromagnets, the magnetization of the microscopic region is still zero. [7]

3.4.2 Thin films

In the case of thin films on a substrate, it is possible for the intrinsic magnetic properties such as magnetization or Néel temperature to differ from same material in bulk form. [12]
There are two main reasons for the change in properties of the magnetic material. The first one may be the special environments of surface and interface atoms. The second possible reason is the strain caused by the substrate, more precisely, illustrated by some mismatch of lattice constant which leads to piezomagnetism. [12]
Also, the lattice parameters of a perfectly relaxed film are not the same as parameters of the bulk material.

4. Measurements

4.1 Devices and material used in measurements

MOKE

For MOKE measurements, we used a closed system of cryostation with small vibrations from Montana Instruments, see the picture 4.1.
The light could enter by custom quartz (homosil) windows which are transparent in broader spectrum than classical quartz glass, including also UV.
To lower the temperature in the system, the system used Helium. The cryostation has HiVac operation which permits us to lower the temperature and omit formation of the ice coating on window. HiVac and heater assure high stability.
The source of the external magnetic field was an electromagnet which produced either in-plane or out-of-plane field to the sample based on the position of our sample. The magnetic fields magnitude was dependent on pole shoes and could supply up to 900 mT.

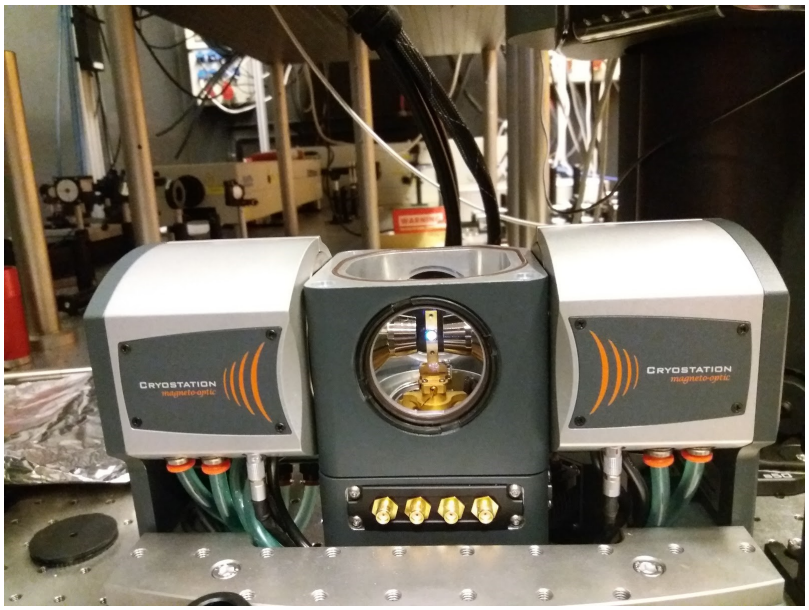

Figure 4.1: Cryostation with a sample. The field is applied IP, detection is done OOP.

The sample was attached on adapter with Leitsilber 200 Silver paint from TED PELLA INC. (Lot.No.: 114757-114).
The source of light was a wide spectrum laser driven lamp with declared stability under 1% which was needed for precise measurements. For normalizing to the incoming amplitude from lamp, we used model SR830 DSP lock-In amplifier from Standford Research Systems, chopper and diod which registered the intensity of the light.
We also used polarizer and rotating analyzer and mirror. The polarizer separated s and p polarizations and p polarization was reflected from the mirror, while the s polarization continued towards the sample. The polarizer and the analyzer were made from wide spectrum BBO crystals.

The custom made measuring program was able to measure the Kerr rotation which was calculated according to equation 2.19. In this custom made program, we could adjust the number of accumulations, the values of relative angles of rotating analyzer we want to measure.
For the measurements, we used Andor spectrometer with CCD camera which allowed us to get high spectral accuracy. Also, using this spectrometer combined with the method of rotating analyzer, we are able to register wide range of spectrum at once.
We analyzed the measured data by using Origin program from Origin Lab.

Ellipsometry

In another type of our measurements, we used the ellipsometer (model RC2) combined with analysis program CompleteEASE from company J.A.Woolam. The RC2 model is an ellipsometer with dual rotating compensators which is capable of determining all components of Muller matrix. The Muller matrix is an equivalent of Jones matrix but for unpolarized or partly polarized light.
We analyzed the measured data by using Origin.
For temperature dependent measurements, we used a cooling device and Peltier element (figure 4.2) to which we attached the sample by using the same silver gel as in our MOKE measurements. With the Peltier element, we could heat up the sample up to almost $120°C$. We used the cooler to be sure we do not damage the ellipsometer during the measurements when the temperature was high. The Peltier element was attached to the cooling device by using clamps, as shown in figure 4.2.

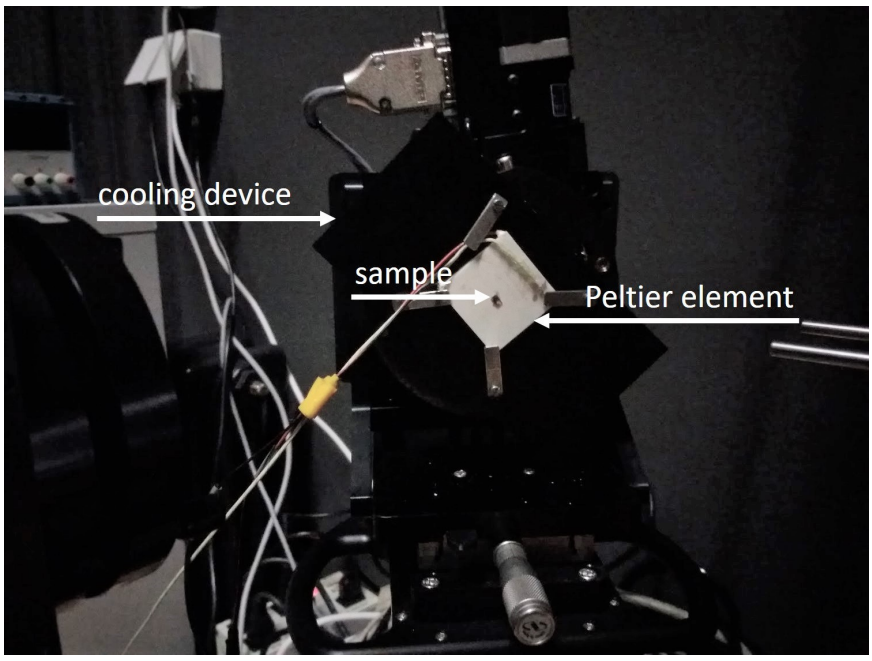

Figure 4.2: The sample of Mn_3GaN thin film on STO substrate glued on a Peltier element during ellipsometric measurements.

Cleaning of the sample

For cleaning the sample from the silver paste or other impurities on the surface of the sample, we used acetone, ethanol, isopropyl alcohol, distilled water and compressed air.

Other devices

We also used an Olympus polarizing microscope (model DP27) to visualise the surface of our samples. The microscope is equipped with dual polarizers and as such can also detect contrast induced by Kerr effect on magnetic domains.

4.2 The basics of measurements

As we have already mentioned, the motivation of the study of antiferromagnets was mainly because of the fact it might be used as a memory storage device.
For that reason, we used various thin films of antiferromagnets on substrates fabricated at Imperial College, London.
The antiferomagnets were metalic antiperovskites which have cubic crystal structure and formula M_3AB, where A and B stand for cations and M for a magnetic element and also, huge Kerr effect was registered on similar material in previous studies.
As written previously, our samples exhibit a piezomagnetic effect, see the figure 1. Therefore by applying the same amplitude of the field with opposite direction, a net magnetization would change its direction according to the theoretical ab-initio calculations (performed by Jan Zemen).
More specifically, the majority of the samples we used were Mn based antiperovskites which have two possible magnetic structures: Γ^{4g} and Γ^{5g}. Both possible configurations of the spins in the plane [111] of the cubic cell are depicted in the figure 4.3.

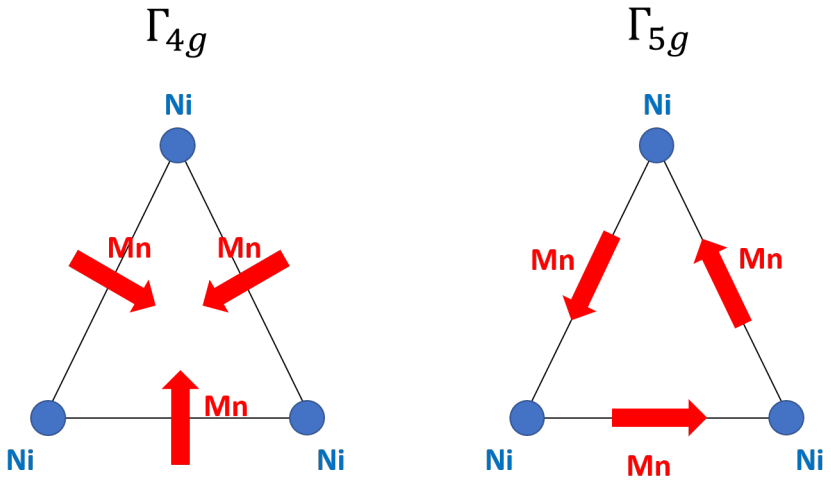

Figure 4.3: Possible configurations of Mn based antiperovskites: Γ^{4g} and Γ^{5g}

In the case of Γ^{5g}, we are not able to measure any MOKE signal because of the symmetry. This is caused by the fact that only some off-diagonal components of the permittivity tensor (see the equation 2.13) contribute to MOKE measurements for the light of incidence perpendicular to the surface.
Contrary to that, Γ^{4g} configuration with canting of the local Mn moments because of the strain, showed us that it could be potentially registered in MOKE measurements. The mentioned strain was caused by the slight lattice mismatch between the thin layer and the substrate.
Fortunately, it seems that our samples are containing mainly Γ^{4g} configuration, as measurements of Anomalous Hall effect (AHE) in the article from Boldrin et al. [30] and our MOKE measurements showed some results.
The lattice strain causes the change in canting of the local Mn moments.
There are two opposite directions as we had substrates with smaller and bigger lattice constant than the antiferromagnetic layer: Mn_3NiN on LSAT and STO. Therefore, we presume tensile and compressive strain, producing net magnetization with the opposite direction, see the figure 4.4.

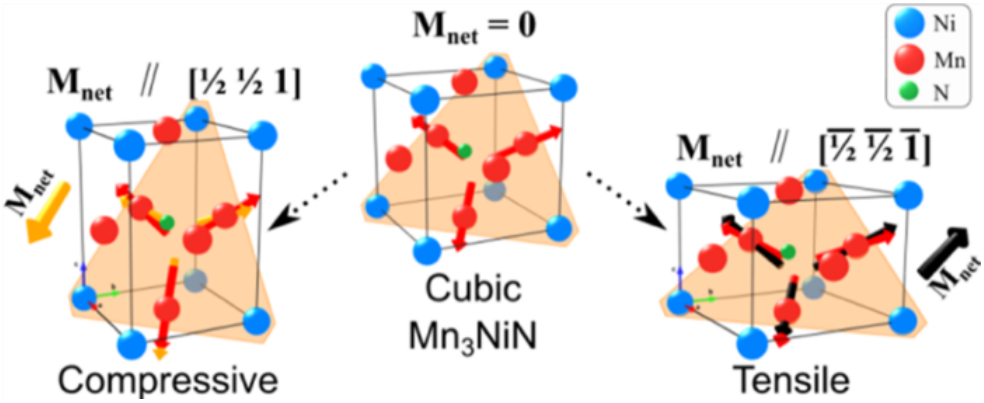

Figure 4.4: The effect of compressive and tensile strain on the net magnetization of Mn based antiferromagnetic material and zero net magnetization for the material without any strain, from [11]

As we mentioned before, the antiferromagnetic material might have several magnetic configurations.
Our sample's two possible configurations, which are called "in" and "out", are depicted in the picture 4.5, also with two polarities of the external magnetic field.

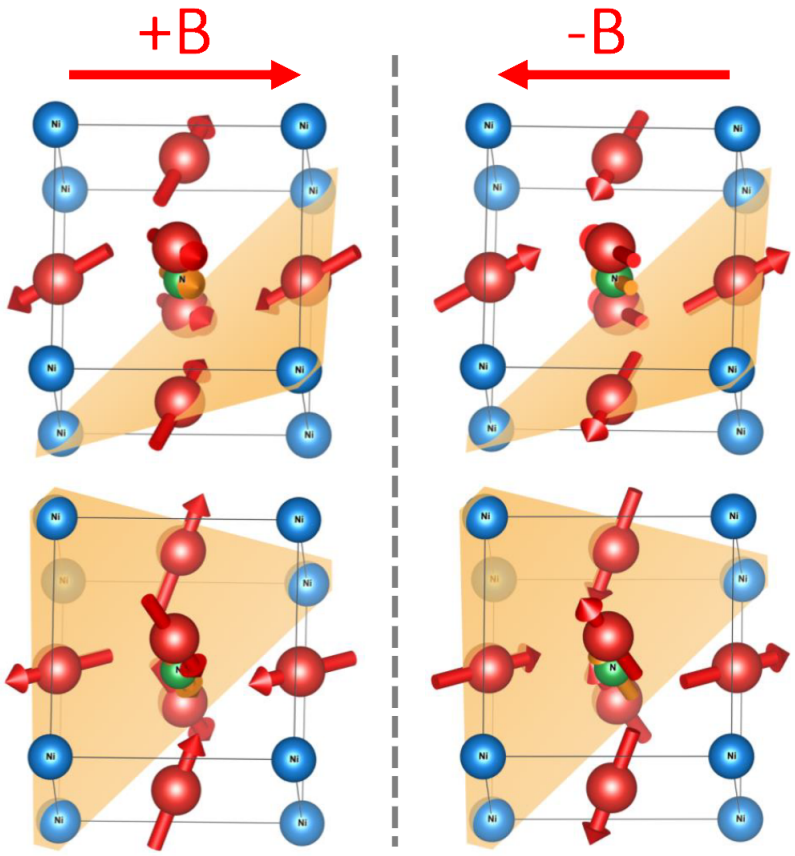

Figure 4.5: Two possible configurations, "in" (on the left side up and on the right side down) and "out" (on the right side up and on the left side down), with both polarities of the external magnetic field. If the two types of domains were in equilibrium, no MOKE could be measured. Courtesy of Jan Zemen.

Samples

Our samples were thin antiferromagnets on substrates prepared at Imperial College in London, UK. The material was grown in [100] direction. Namely, we measured on:

- thin film of Mn_3NiN on LSAT $(LaAlO_3)_{0.3}(Sr_2TaAlO_6)_{0.7}$ substrate
- thin film of Mn_3NiN on STO $SrTiO_3$ substrate
- thin film of Mn_3GaN on STO substrate.

The morphology pictures from polarizing microscope for Mn_3NiN on LSAT and STO are in the pictures 4.6 and 4.7.
We tried to visualize the magnetic domains through the microscope but we did not see any. Therefore, eventual ferrimagnetic and antiferromagnetic domains are below the resolution of the microscope or nonexistent.

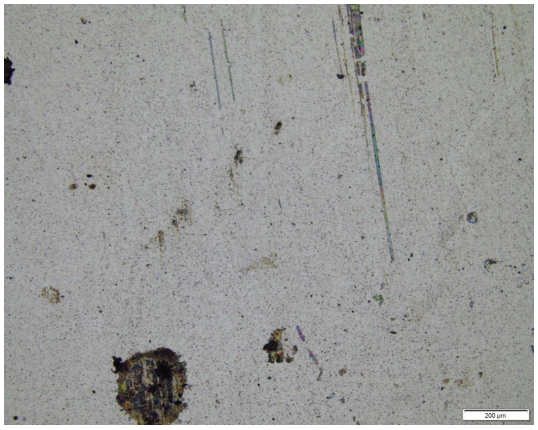

Figure 4.6: Thin layer of Mn_3NiN on LSAT under polarizing microscope. We can see that the surface has some impurities.

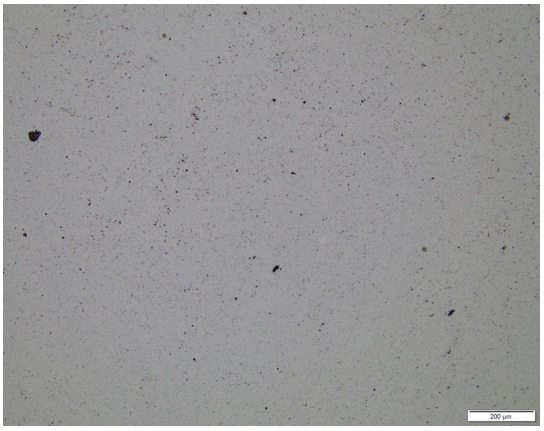

Figure 4.7: Thin layer of Mn_3NiN on STO under polarizing microscope

4.3 MOKE measurements of Mn_3NiN thin films

We studied MOKE in nearly normal incidence (OOP field having the highest sensitivity) while applying IP magnetic field on two samples, both with Mn_3NiN thin films [100] grown on a substrate with a lattice mismatch. We could apply IP field thanks to the magnetic moments being in 45° to the surface (see the picture 4.4). We chose this configuration because IP field does not require a beamsplitter as OOP does and therefore in our case, the spectral range is not reduced.
We obtained the dependence of Kerr rotation θ_K for two samples of thin layer of Mn_3NiN on different substrates (LSAT and STO).
The two subtrates created different strain in the samples, tensile and compressive, which is visible in data from Imperial College presented in the table 4.1.
The Néel temperature of the antiferromagnetic layer should be around 245 K, which is also visible from the graphs depicted in the figure 4.8 and 4.9 measured at Imperial College, as the peak in magnetization is around this temperature.
Various protocols were used. In ZFC (zero field cooling), the magnetic moment starts to be measured after we lower the temperature, while increasing the temperature.
In FCC and FCW, at first we cool down the sample with already applied external field of 50 mT.

	XRD	calculated	$\epsilon_{xx} = \epsilon_{yy}$
Mn_3NiN	c(Å)	a(Å)	(%)
STO 20 nm	3,8977	3,8735	-0,18
LSAT 50 nm	3,8654	3,8867	+0,16

Table 4.1: X-ray diffraction results from [11] for the samples of Mn_3NiN thin films. The a lattice parameter is calculated from the c lattice parameter determined from XRD and the measured Poisson ratio $\nu = 0{,}41$. We can observe a different strain for the two substrates. The values next to the name of the substrate in nm indicate the thickness of antiferromagnetic layer.

FCC stands for field cooled cooling, which means that data is measured during the cooling.
FCW protocol used only for the sample with STO substrate stands for field cooled warming, which means that the measurements is carried out during the heating of the sample (after being cooled down).
Graphs 4.10 and 4.11 show the magnetization curves of two samples, both with Mn_3NiN thin layer but on different substrates. We can see that the coercive field increases with lower temperature which means that the sample at lower temperatures should be able to tolerate higher external magnetic fields without being depolarized.

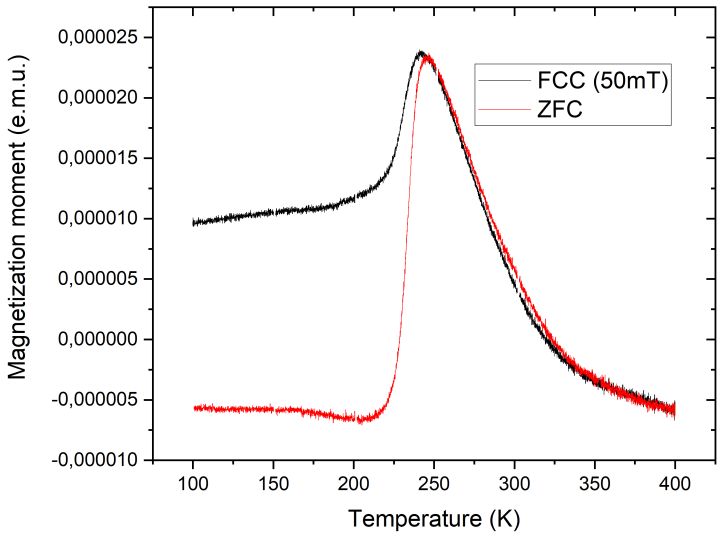

Figure 4.8: Dependence of magnetization moment on temperature in Mn_3NiN on LSAT. We can see a peak in magnetization roughly around 245 K. Courtesy of Imperial College.

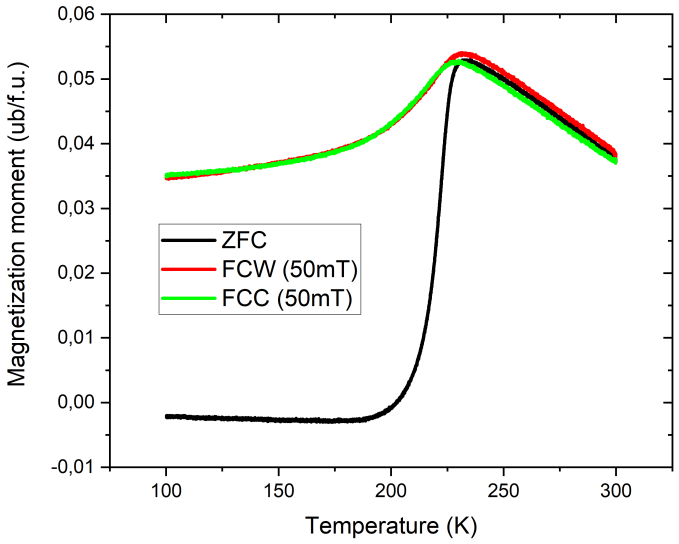

Figure 4.9: Dependence of magnetization moment on temperature in Mn_3NiN on STO. We can see a peak in magnetization roughly around 245 K. Courtesy of Imperial College.

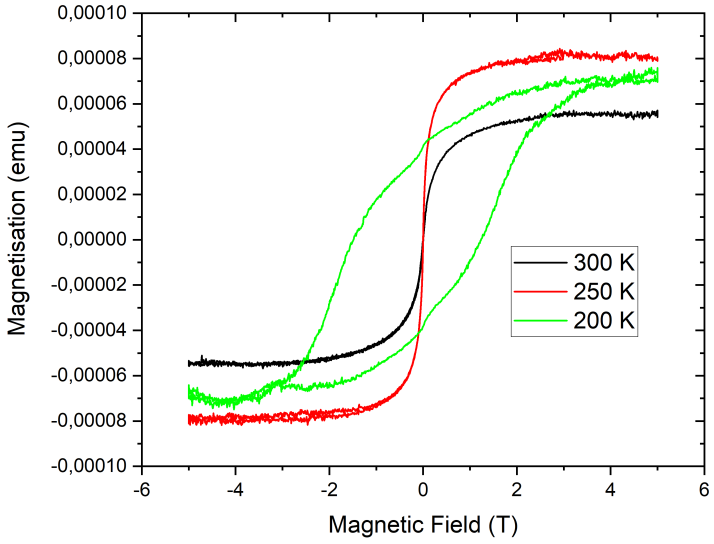

Figure 4.10: MB graph for Mn_3NiN on LSAT, courtesy of Imperial College

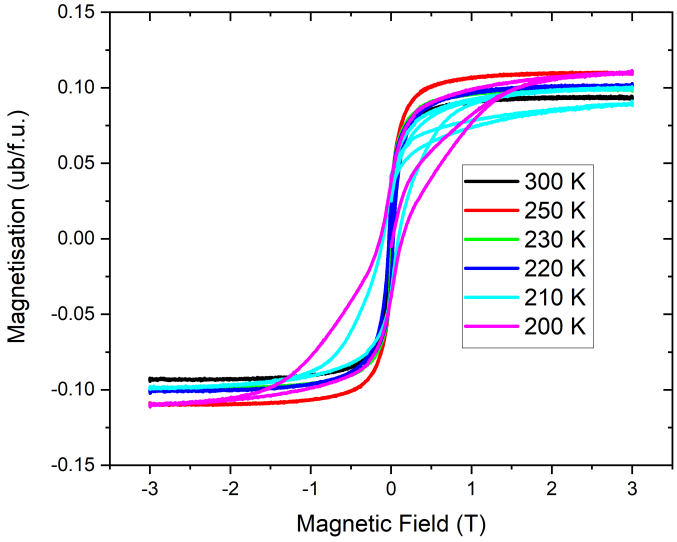

Figure 4.11: MB graph for Mn_3NiN on STO, courtesy of Imperial College

In the graph 4.12, we show the measured data of Kerr rotation for the sample of Mn_3NiN thin film on LSAT substrate as a function of various energies of light. In the same graph, we show also the ab-initio theoretical values with strain induced and values scaled so that they match the MOKE amplitude. The graph 4.13 depicts the same thing for the second sample of Mn_3NiN thin film on STO substrate. The theoretical values roughly match the measurements in both graphs (4.12 and 4.13).
The Kerr rotation depicted in these graphs is an average of the measurements in two polarities of the external magnetic field. Practically, we did the difference of the measured Kerr rotation for the two polarities of the external field and divided it by two.
During the measurements, the sample was at room temperature (supposed above Néel temperature) in the cryostation when an external field was applied. After that, the sample was cooled down in field and several measurements were done for various values of temperature. Then we heated up the sample and applied the other polarity of external field.
As we can see from the graphs 4.12 and 4.13, measured around or below room temperature in cryostation, LSAT has a positive amplitude of Kerr effect, while STO has a negative one even though they had been measured by same method. The samples show opposite MOKE while having same magnetization behaviour and Néel temperature. Therefore, we can conclude that the opposite sign of Kerr effect from the tensile and compressive configurations of Mn_3NiN summed up in table 4.1 and is in accordance with our previous assumptions and theoretical calculations.
The difference in noise in graphs 4.12 and 4.13 is due to different measurement parameters.

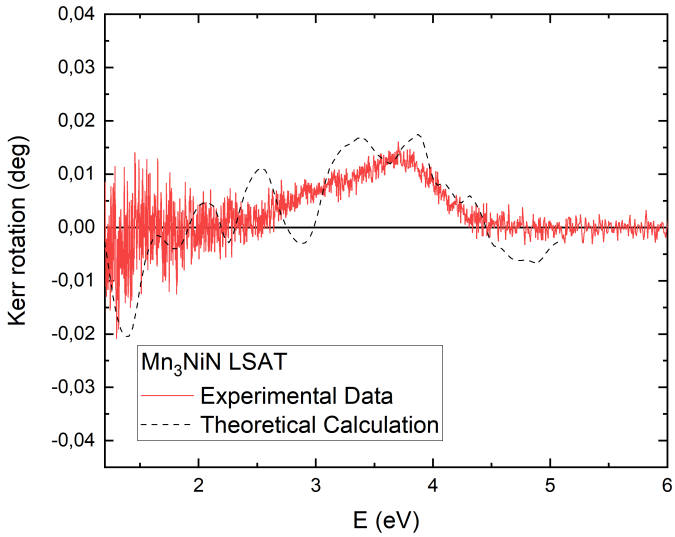

Figure 4.12: Thin film on LSAT substrate has a positive amplitude of Kerr effect. Courtesy of Jan Zemen for the scaled theoretical ab-initio calculations.

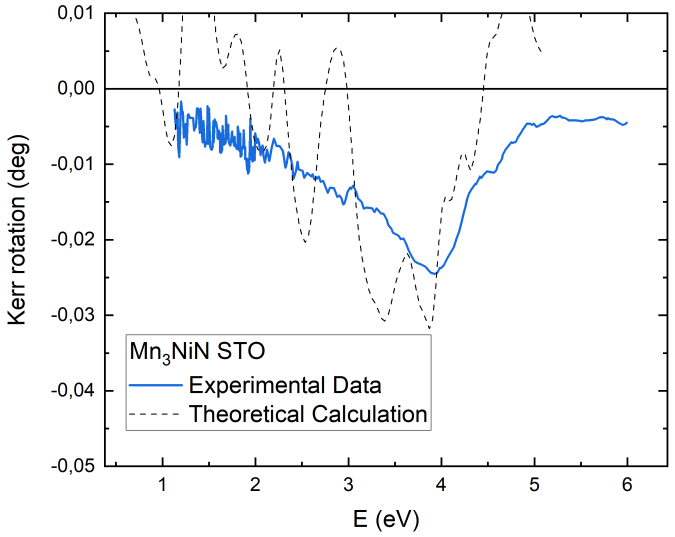

Figure 4.13: Thin film on STO substrate has a negative amplitude of Kerr effect. Courtesy of Jan Zemen for the scaled theoretical ab-initio calculations.

To observe Kerr effects with two opposite signs for two samples of different strain for one set of samples and measurement runs, does not directly mean that what we register was the net magnetization of the samples. There possibly could be change in the magnetic domain structure in time or other effects which could make the MOKE measurements unreliable even though we once obtained reasonable data.
For example, if the ”in” and ”out” domains depicted in the figure 4.5 were in equilibrium, we would not be able to measure any MOKE signal. Also, the mag-

netic ordering in the sample is uncertain and we did not obtain any data from XRD or magnetometry. Another complication is the canting of the spins by 45°. Therefore, bigger statistics is needed.
To get the statistics and verify the method with cooling in applied field and also to observe a magnetic phase transition, we conducted some other similar measurements. This time, the measurements were done with sample at various temperatures. Heating above 245 K, we should get to paramagnetic phase of the material. Before, the samples were straight from high field measurements.
The results can be seen in the graph 4.14 for the sample with LSAT substrate and in the graph 4.15 for STO substrate. The external magnet field was switched after cooling to 230 K.

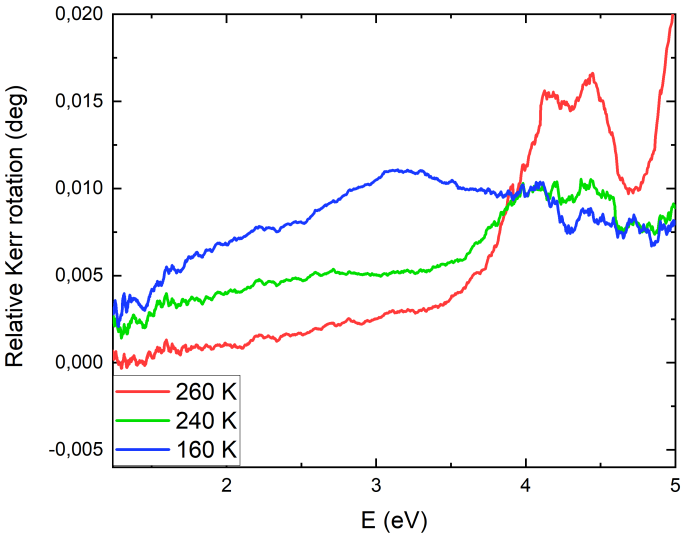

Figure 4.14: Relative Kerr rotation at various temperatures for Mn_3NiN thin film on LSAT.

We can see the expected gradual change of Kerr rotation with the change of the temperature of the sample for the sample with STO substrate. Also, the Kerr rotation under the Néel point corresponds to previous measurements depicted in graphs 4.12 and 4.13.
In the graph 4.14, we depicted relative Kerr rotation. It means that we subtracted any possible effect coming from the glass. We did it thanks to one additional measurement at room temperature and without the front glass of the cryostation. We observe a change around 4 eV with the change of temperature.
Also, the peak in Kerr rotation around 4 eV registered for the temperature of 340 K is ten times smaller in magnitude for the measurement with the sample (graph 4.15) with STO substrate than we observed otherwise. However, this happened after several cycling of the temperature. The change in Kerr rotation around 4 eV is gradual according to temperature in the case of STO substrate.
This was not the only measurement where some problems occurred. In the graph 4.16 for the sample with STO substrate, the Kerr rotation does not change gradually with temperature. Due to the method there is a shift (dependent on the right crossing point of the polarizers), meaning there might be an offset.

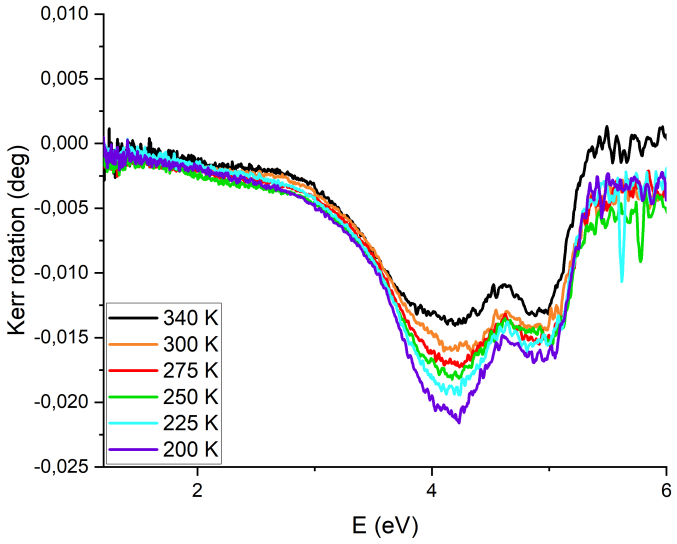

Figure 4.15: Kerr rotation at various temperatures for Mn_3NiN thin film on STO.

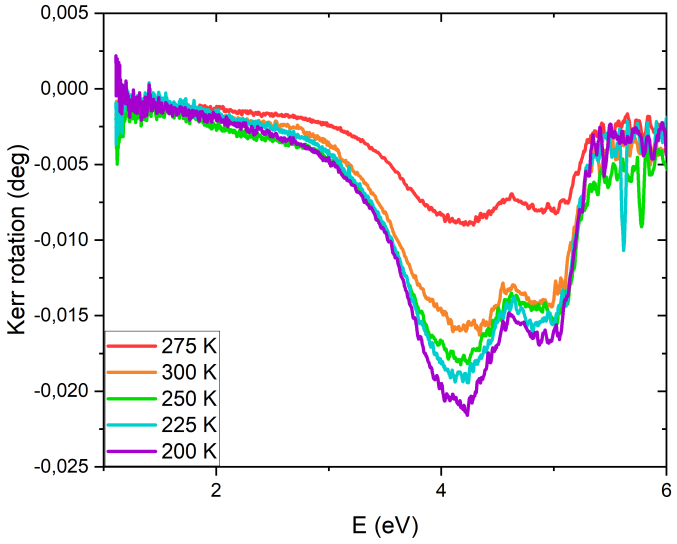

Figure 4.16: Kerr rotation at various temperatures for Mn_3NiN thin film on STO.

Therefore we repeated the measurement. The results in the graph 4.17 correspond to the previous results in graphs 4.12 and 4.14. Still, we did not observe a change in peak around 4 eV with change of the temperature which we expected because of the known value of Néel temperature. Another measurement of the sample with STO substrate, gave us a spectra (see the graph 4.18) which does not match the previous sign of the Kerr effect (graph 4.13). The minimum around 3 eV could be explained by the oversaturation of the detector.
We checked if the calculations were consistent and did not register any possible

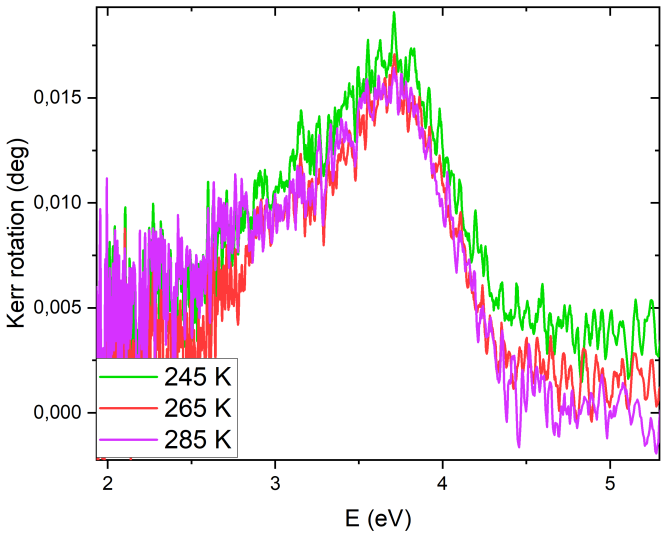

Figure 4.17: Kerr rotation at various temperatures for Mn_3NiN thin film on LSAT. Small signal in the UV range could be explained by misalignment of the detector or degradation of the surface.

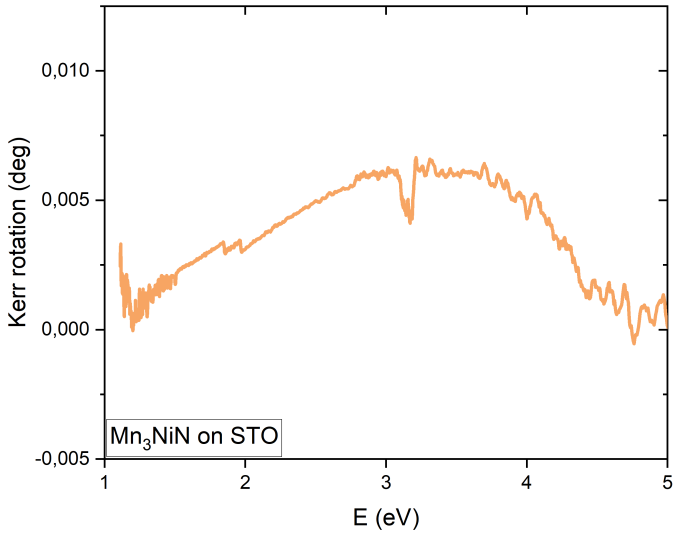

Figure 4.18: Kerr rotation for Mn_3NiN thin film on STO at 235 K. The sign of the measured Kerr effect does not match the previous measurements. The dip around 3 eV could be explained by the oversaturation of the detector.

problem. Therefore, one of the possibility to explain this reverse of the sign of Kerr effect could be that we have actually two configurations (see the figure 4.5) in the sample which can form.
The ambivalence of our MOKE results could be explained by the improper domain population. There are domain configurations that result in different net magnetization vector of the sample, meaning different MOKE sign measurements, see

the picture 4.5. The ratio of the two types of domains depicted in the picture 4.5 and not the strain would determine the sign of Kerr effect if this hypothesis was true.
We measured the data for two polarities of the external field, observing two opposite amplitudes of Kerr effect. The MOKE spectra depicted in the graphs are the result of averaging the value of three consecutive measurements.
The possible change in domains of the material could cause also the change in magneto-optical parameters of the sample which would explain why we measured something different each time.
Other possibility is in the method where we apply the external field for a long time. To verify this assumption, we checked the time stability of the signal to see if the sample is changing during measurements (as we see domain might be there and might have and effect as we do not saturate).
We did several consecutive MOKE measurements in time of the two samples with Mn_3NiN thin layer for two temperatures: 235 K and 300 K (under and above Néel temperature). This means that we did several measurements for one constant temperature (from 7 to 9 measurements) for each polarity of the external field.
The figures 4.19-4.23 depict the time development of Kerr rotation for various energies (1,5 eV, 2 eV, 2,5 eV, 3 eV and 3,5 eV) at constant temperature. We show Kerr rotation for two polarities of external magnetic field separately (negative and positive).
It the graphs 4.19-4.23, we see the evolution of Kerr rotation at one energy for one constant temperature. We see the increasing trend in the data for 235 K, while the data for 300 K is stable, the relative variation is under 1%. Therefore, we can say that for the temperature of 235 K, the Kerr rotation is not the same for all measurements but increases in time. However, for 300 K measurements, the situation is different as the value of Kerr rotation does not vary significantly. Seeing that the trend of Kerr rotation is similar for all five values of light energies, we can say that a change of the data for 235 K is in the whole spectrum.
As we mentioned before, Néel temperature of Mn_3NiN thin film should be around 245 K. Therefore, for each temperature, the material was in a different magnetic phase. For 235 K, it was in antiferromagnetic phase, while for 300 K, the sample should already be in its paramagnetic state but it still shows some effect. Therefore, it might be still partially ferromagnetic. However, this should not interfere with the antiferromagnetic phase and behaviour.
Note also, that the evolution of Kerr rotation in time for 235 K has very similar trend for both polarities so we could think that by making the difference of the two and dividing it by two, we could probably get the same value of Kerr rotation. Nevertheless, the previous measurements seemed to contradict this assumption. The measurement of Kerr rotation is not precisely reproducible because of the time dependence of the measurement (see the graphs 4.19-4.23), probably caused by domain dynamics.
To conclude, from several measurements of Mn_3NiN thin film on two substrates with different strains coming from lattice mismatch we performed, we observed a dependence of magneto-optical properties of the antiferromagnet on the strain (graphs 4.12 and 4.13). We also registered a change in Kerr rotation with change of the temperature of sample (for example graph 4.17). However, after performing

several measurements, we observed an ambivalence in our results (if we compare for example graphs 4.13 and 4.18). Also, the change of Kerr rotation with change of temperature was not always gradual.
Therefore, we performed time-dependant measurements (graphs 4.19-4.23) which showed time evolution of the Kerr rotation in whole spectrum under the Néel point.

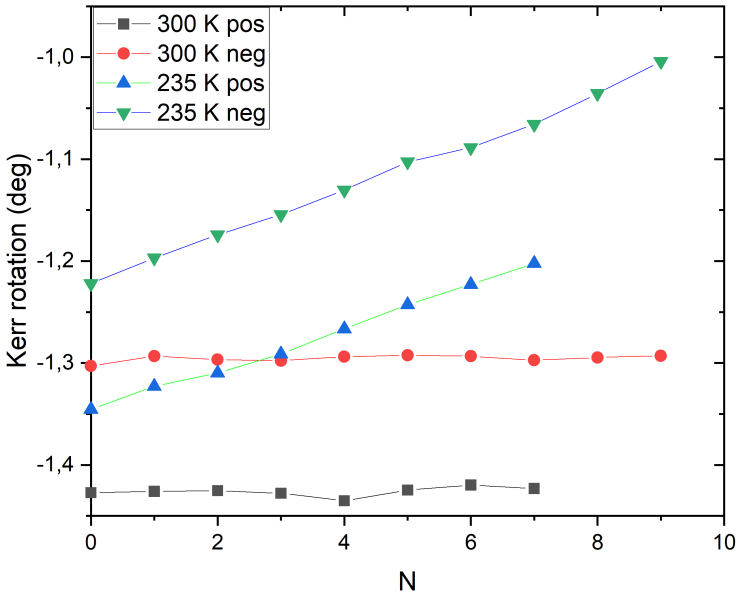

Figure 4.19: The change of measured Kerr rotation in time. The measurements done for Mn_3NiN thin film on LSAT substrate for constant temperatures 300 K and 235 K, light energy at 1,5 eV.

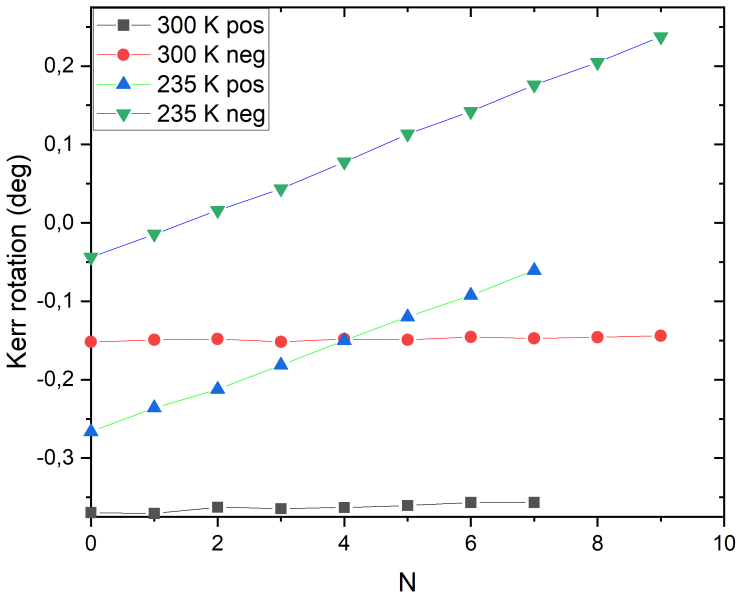

Figure 4.20: The change of measured Kerr rotation in time. The measurements done for Mn_3NiN thin film on LSAT substrate for constant temperatures 300 K and 235 K, light energy at 2 eV.

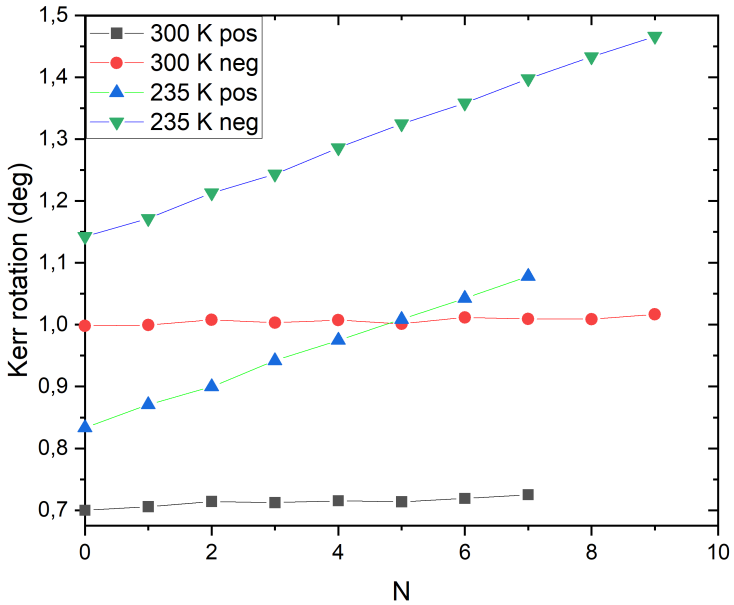

Figure 4.21: The change of measured Kerr rotation in time. The measurements done for Mn_3NiN thin film on LSAT substrate for constant temperatures 300 K and 235 K, light energy at 2,5 eV.

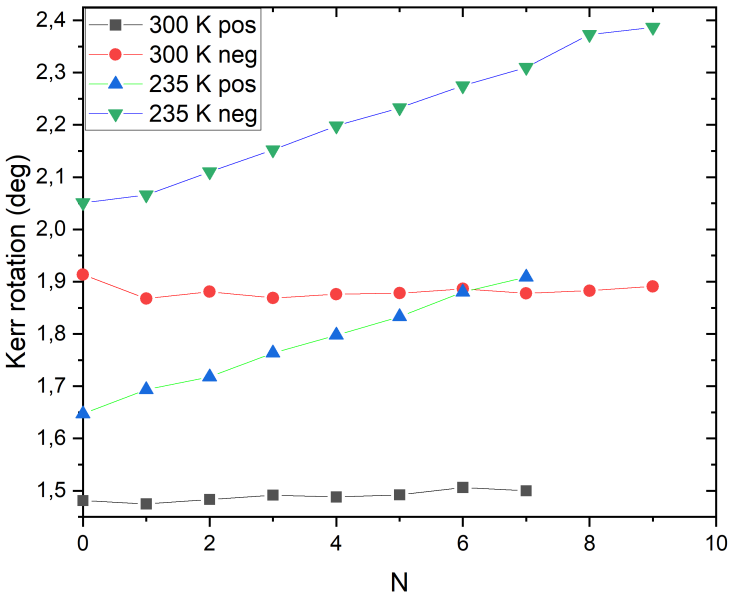

Figure 4.22: The change of measured Kerr rotation in time. The measurements done for Mn_3NiN thin film on LSAT substrate for constant temperatures 300 K and 235 K, light energy at 3 eV.

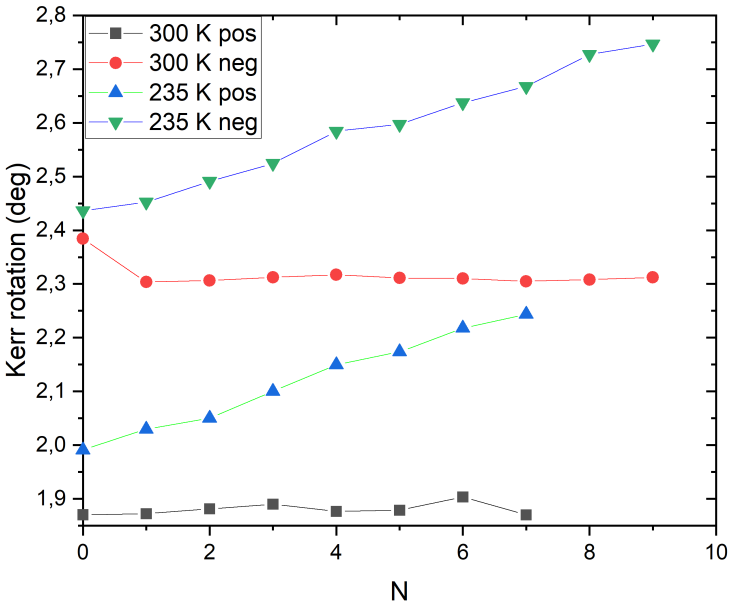

Figure 4.23: The change of measured Kerr rotation in time. The measurements done for Mn_3NiN thin film on LSAT substrate for constant temperatures 300 K and 235 K, light energy at 3,5 eV.

4.4 Ellipsometry measurements

In the ellipsometry measurements, we studied the sample of the thin film of Mn_3GaN on STO at room temperature for two different angles of incidence.
This antiferromagnet was chosen as it has same stucture as Mn_3NiN we previously used in our MOKE measurements. Currently, we could not use Mn_3NiN using our ellipsometry measurements because we measure at ambient air and therefore the attainable temperatures are from around $20°C$ to $120°C$.
The reason why Mn_3GaN is a good candidate for these measurements is that its Néel temperature is above room temperature.
To do the measurements, we used an ellipsometer with rotator which is usually used to see anisotropy of the sample. More specifically, we used this method to see if there is an anisotropy at the surface and also to see if this changes with increasing temperature.
The anisotropy is visible from the measured spectra.
We always chose data for an energy of light of 1,5 eV as the material has low depolarization at this light energy, see the graph 4.24 which shows a depolarization for one of the measurements for Mn_3GaN thin layer. This measurement is discussed later in this chapter.
The graph of optical constants, also for the same measurement is shown in graph 4.25 for reader's information.

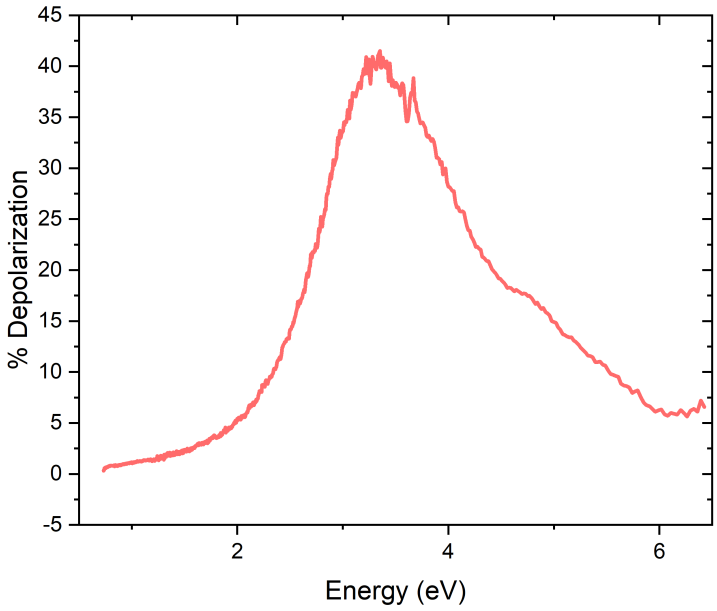

Figure 4.24: Depolarization during measurements for Mn_3GaN thin film at $120°C$. The angle of incidence of light was 60°.

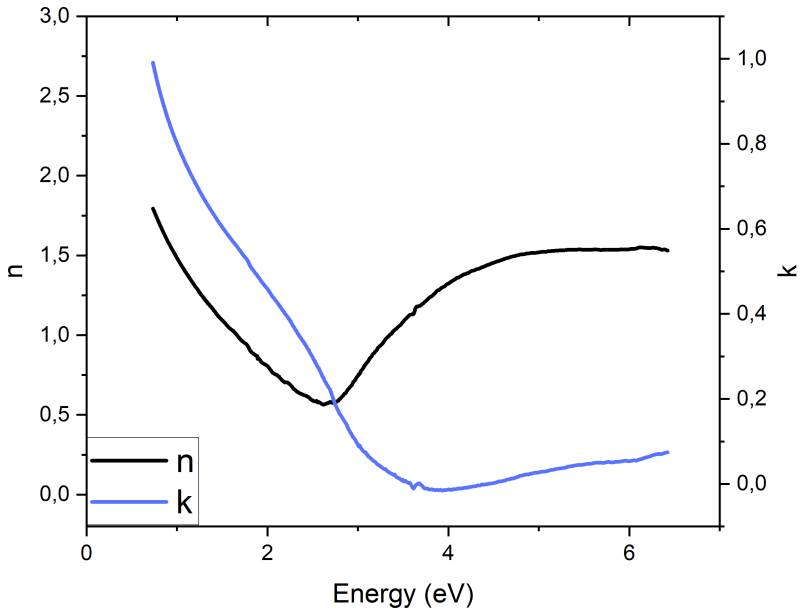

Figure 4.25: The optical parameters during measurements for Mn_3GaN thin film at 120°C. The angle of incidence of light was 60°.

We thought that a passage to a ferrimagnetic phase is possible above Néel point because of the alignment of the canted moments, see the picture 4.26.
This transition ought to be registered in the ellipsometry measurements as it has different symmetry than the antiferromagnetic phase.

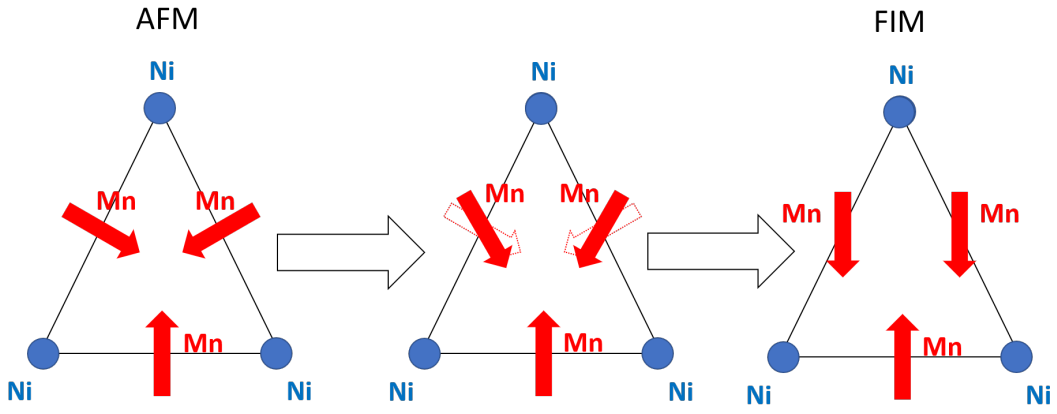

Figure 4.26: Possible transition from antiferromagnetic phase to ferrimagnetic phase of the sample for the temperature above Néel point. The previously canted moments align.

For 65°, we observed spatial dependence of Ψ, while for 45°, the dependence was more even, see the graph 4.27.
From that we thought that the symmetry might be changing with different angle of incidence, as there is a different projection to the net magnetization vector. We observed the anisotropy in the orientation.

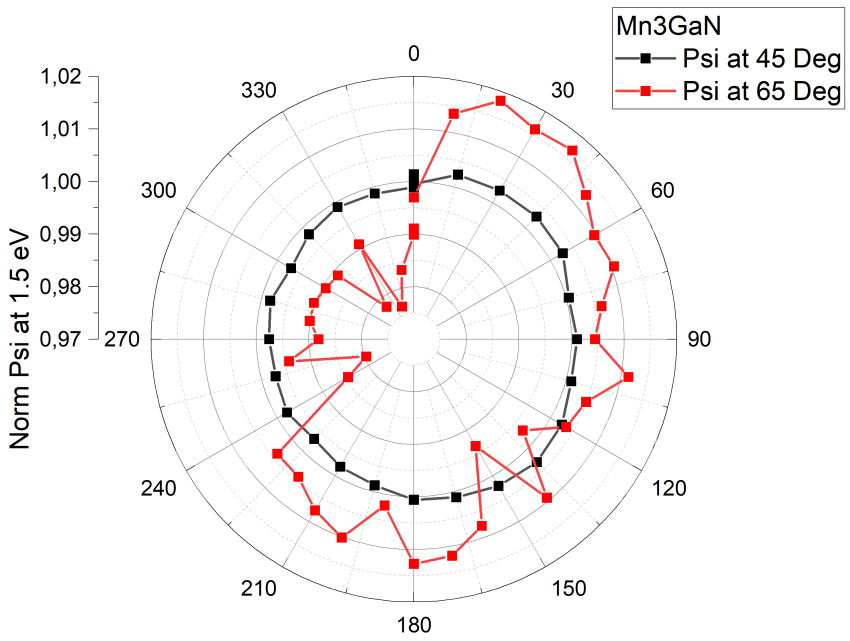

Figure 4.27: The ellipsometry measurements for thin film of Mn_3GaN on STO. Ψ for two incidence of light at room temperature.

For measurements above Néel point, we also used the sample of Mn_3GaN thin film on STO substrate.
We glued the sample on Peltier element by using silver gel. The Peltier element was then put on a cooling element and all this was attached to the rotator in ellipsometer, see the picture 4.2.
We increased the temperature of Peltier element and sample by using current control with current supply. The current was increased by smaller steps, so that we do not exceed the maximal temperature of 120°, up to approximately 84°C which is around the value of the Néel temperature of this material. As we can see from the graph 4.28, with temperature around the Néel temperature, the spatial dependence remained almost the same, only small maxima arose in the place of minima.
We tought that in order to observe more visible evidence of the transition of this antiferromagnet to different magnetic state, especially to be sure we have transitioned to paramagnetic state of the material, we would have to increase the temperature to higher values. Therefore, we repeated the measurements but heated the Peltier element to maximum.
We measured for the rotation of rotator from 0° to 360° à 5° for two angles of incidence: 45° and 60°.
To focus the light only on the sample, we used an aperture as the surface of the sample was small enough to not come of the edges of the sample but still big enough so that the reflected light has intensity high enough to be registered by the detector.
At first, we verified that while rotating the sample, light illuminates the sample approximately at the same location. We did that by gradual adjustments of the sample at various angles of rotator.

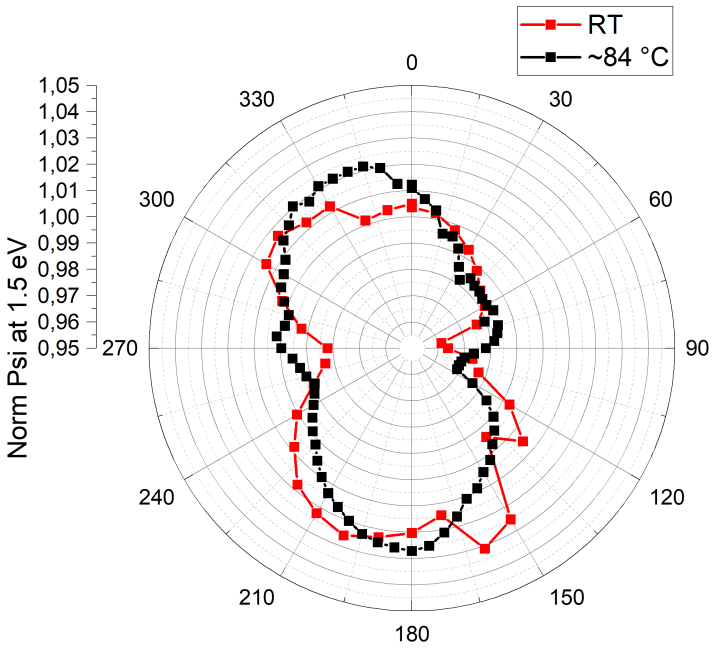

Figure 4.28: The ellipsometry measurements for thin film of Mn_3GaN on STO. Ψ for two incidence of light at room temperature and at $84°C$.

First measurements were done at room temperature, $T_R \sim 24°C$. After averaging the measurements around 1,5 eV and subtraction of supposedly thermal drift (see the graph 4.29), we get the spatial dependence for the angle of incidence 60°. We assume that the evolution depicted in graph 4.29 is thermal drift because the measurements take hours and we might not have any other way to ensure that we measure still with the same parameters set up.

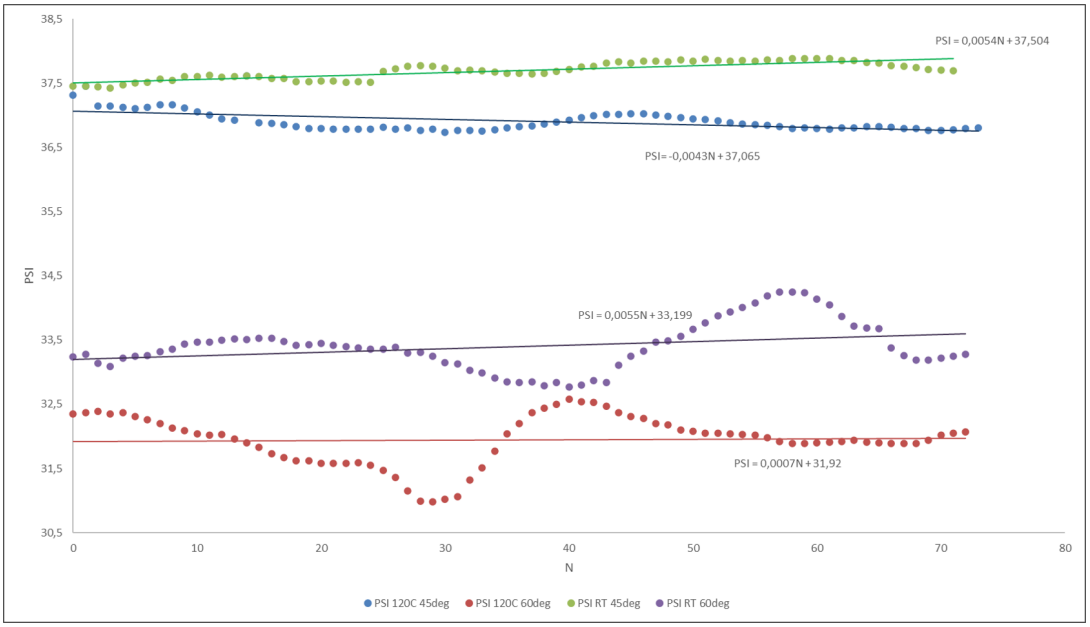

Figure 4.29: The thermal drift of the ellipsometry measurements.

We again augmented the temperature of the sample thanks to the Peltier element. With electric current around 1,4 A and under voltage of approximately 9 V, we got to temperature around $T_1 = (116 \pm 3)°C$.
Again, we subtracted the slight temporal temperature drift and averaged the three measurements around 1,5 eV, for the angle of incidence 60°. In the graph 4.30, we plotted normalized value of Δ for room temperature and for T_1. In the graph 4.31, the value of normalized Ψ is depicted the same way as was Δ before.
From graphs 4.30 and 4.31, we concluded that we had probably done a mistake in between the measurements by rotating the sample and therefore a rotation of data by 45° is needed.
We constructed a modified graph for Δ at the angle of incidence of light equal to 60°, graph 4.33, where the data for higher temperature were shifted by 45°.
We can see that we did not succeed to register a magnetic phase transition.
While we see some changes, there is not a visible large change that could be attributed to the transition between antiferromagnetic state to the paramagnetic or possibly ferrimagnetic state. Further and detailed investigation is needed to understand the problem and ensure the validity of the measurements and results.

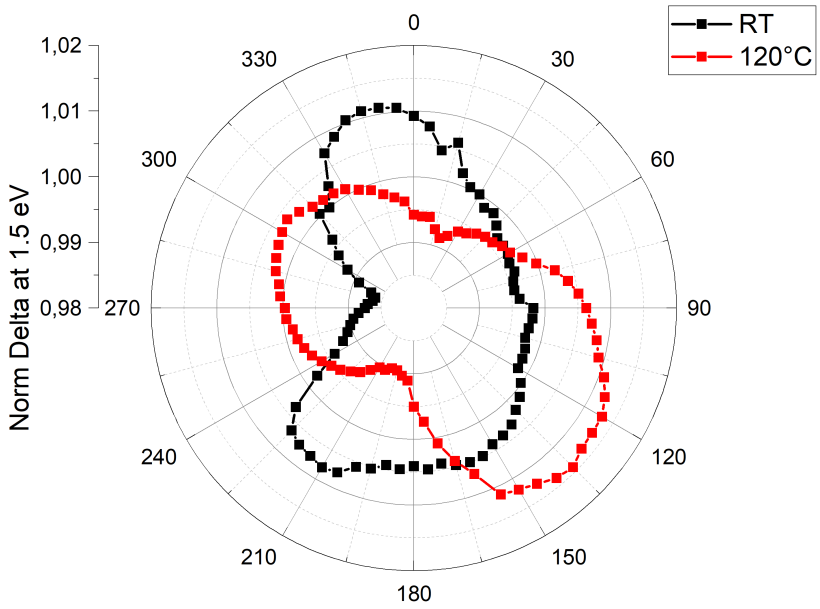

Figure 4.30: Normalized Δ for two temperatures resulting from ellipsometry measurements for a thin film of Mn_3GaN on STO substrate. The angle of incidence was 60°.

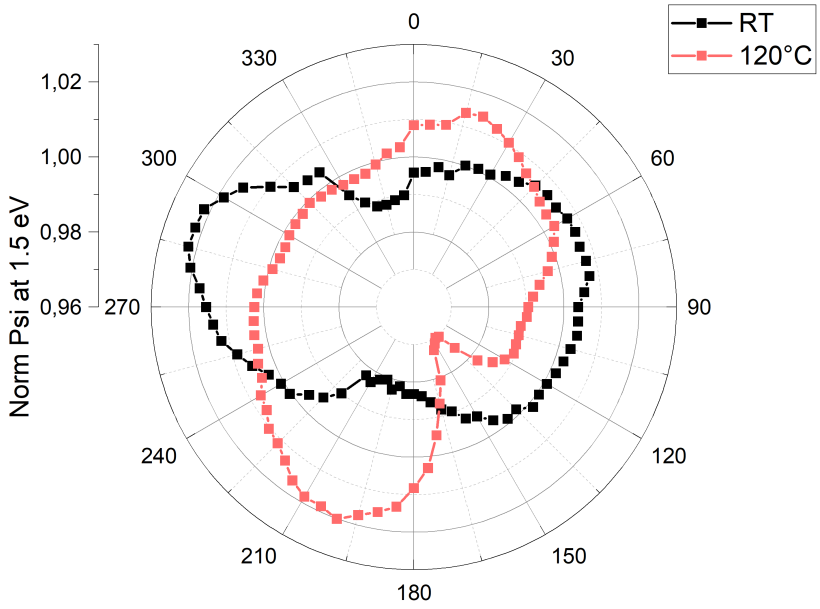

Figure 4.31: Normalized Ψ for two temperatures resulting from ellipsometry measurements for a thin film of Mn_3GaN on STO substrate. The angle of incidence was 60°.

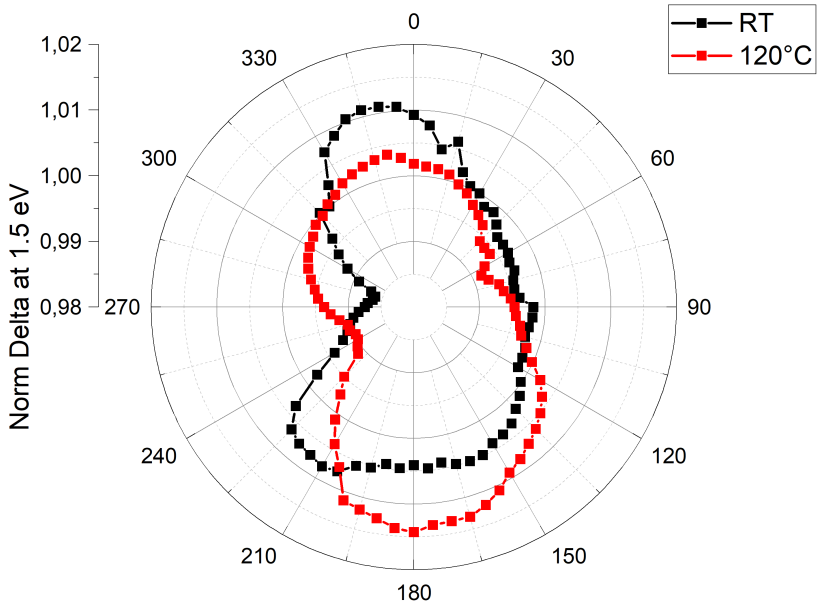

Figure 4.32: Corrected ellipsometry data, normalized Δ. Angle of incidence 60°.

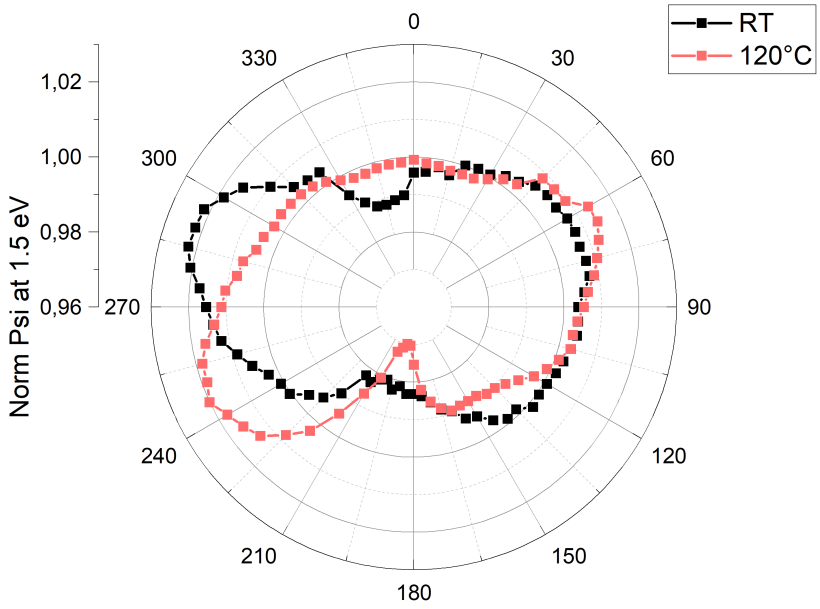

Figure 4.33: Corrected ellipsometry data, normalized Ψ. Angle of incidence 60°.

Conclusion

In this work, we systematically studied optical and magnetooptical properties of noncolinear antiferromagnets Mn_3NiN and Mn_3GaN in the form od thin film. The aim was to measure the spectral dependence of magneto-optical Kerr effect in the investigated samples with respect to the lattice mismatch between the substrate and the antiferromagnetic layer. Based on theoretical calculations the mismatch could create either compressive or tensile strain resulting in appearance of two opposite net magnetizations.

We performed several polar MOKE measurements on thin film of Mn_3NiN on LSAT substrate and STO substrate while applying in-plane magnetic field. The polar MOKE could be acquired due to the spin canting by 45° to the normal plane.

The MOKE spectra showed extreme at around 4 eV with opposite signs of the effect suggesting opposite net magnetization induced by tensile/compressive strain in the samples respectively. That was in agreement with XRD measurements and theoretical predictions. Repeated measurements performed in order to obtain large ensemble of data started to show several discrepancies and large deviations from each other.

Therefore, we performed time dependent measurements for two temperatures: 235 K and 300 K. We observed a time development of Kerr rotation for various light energies at constant temperature, showing that for the antiferromagnetic state at 235 K, the Kerr rotation dynamically changes with time. This effect could be possibly explained by magnetic domain dynamics, resulting in the observed change in magneto-optical parameters for repeated measurements. The argument of domain dynamics is supported by the fact that the sample was not magnetically saturated as the amplitude of the external field was not high enough. Therefore, the domain configuration might differ in each measuremets.

To study the antiferromagnetic/paramagnetic transition and magnetic anisotropy optically, we used ellipsometry measurements. We studied the sample of the thin film of Mn_3GaN on STO from room temperature up to $120°C$ with respect to the in-plane rotation of the sample.

At higher temperatures, we subtracted the thermal drift from the measured data as the data for the rotation of sample at 0° did not correspond to data for 360°. We observed the spatial asymmetry of the measured data caused by crystalline structure.

However, the transition to paramagnetic phase above the Néel temperature could not be observed. We have expected a change of the rotational asymmetry of the data to isotopic state because of the paramagnetic state. Nevertheless, the sample might have a remnant magnetization due to the short-range ordering even above the Néel temperature. This could be the reason why we do not observe the isotopic state in our measurements.

In this thesis, we demonstrated that the magneto-optical spectroscopy can be used to investigate basic physical properties of noncolinear antiferromagnetic materials showing the direction change of net magnetization in investigated samples with respect to the type of strain induced by the substrate. This proved the promising application potential of these materials in novel data storage devices.

Bibliography

[1] T. Jungwirth, J. Sinova, A. Manchon, X. Marti, J. Wunderlich, and C. Felser. The multiple directions of antiferromagnetic spinctronics. *Nature Physics*, 14:200–203, 2018.

[2] M. M. Waldrop. More than Moore. *Nature*, 530:144–147, 2016.

[3] V. Baltz, A. Manchon, M. Tsoi, T. Moriyama, T. Ono, and Y. Tserkovnyak. Antiferromagnetic spintronics. *Review of modern physics*, 90:0034–6861, 2018.

[4] K. Olejník, V. Schuler, and X. Marti. Antiferromagnetic CuMnAs multi-level memory cell with microelectronic compatibility. *Nature Communications*, 8, 2017.

[5] K. Garello, C. O. Avci, I. M. Miron, M. Baumgartner, A. Ghosh, S. Auffret, O. Boulle, G. Gaudin, and P. Gambardella. Ultrafast magnetization switching by spin-orbit torques. *Applied Physics Letters*, 105, 2014.

[6] J. Železný, P. Wadley, K. Olejník, A. Hoffmann, and H. Ohno. Spin transport and spin torque in antiferromagnetic devices. *Nature Physics*, 14:220–228, 2018.

[7] T. Miyazaki and H. Jin. *The Physics of Ferromagnetism*. 2012.

[8] J. M. Daughton and J. S. T. Huang. Magnetoresistive memory including thin film storage cells having tapered ends, U.S.A. Patent 4 731 757, March 1988.

[9] A. Markou, J. M. Taylor, A. Kalache, P. Werner, S. S. P. Parkin, and C. Felser. Noncollinear antiferromagnetic Mn_3Sn films. *Physical review materials*, 2, 2018.

[10] E. V. Gomonaj. Magnetostriction and piezomagnetism of noncollinear antiferromagnet mn_3nin. *Phase Transitions*, 18:93–101, 1989.

[11] D. Boldrin. Giant piezomagnetism in Mn_3NiN. *ACS Appl. Mater. Interfaces*, 10:18863–18868, 2018.

[12] J. Coey. *Magnetism and Magnetic Materials*. Cambridge University Press, New York, 2009.

[13] G. C. Papaefthymiou. Nanoparticle magnetism. *Nano Today*, 4:438–447, 2009.

[14] E. Du Tremolet de Lacheisserie, D. Gignoux, and M. Schlenker. *Magnetism: Fundamentals*. Kluwer Academic Publishers, 2003.

[15] C. Kittel. *Introduction to Solid State Physics*. Eight edition. John Wiley Sons Inc, 2005.

[16] O. Fruchart. Lecture notes on Nanomagnetism. http://fruchart.eu/olivier/lectures/nanomagnetism-2016-11-04.pdf. Accessed: 2020-04-05.

[17] A. Hubert and R. Schafer. *Magnetic Domains: The Analysis of Magnetic Microstructures*. Third Printing. Springer-Verlag, New York, 2009.

[18] J. Schwinger. Nobel lectures in physics 1963–1970, 1972.

[19] P. Malý. *Optika*. Karolinum, 2013.

[20] A. K. Zvezdin and V. A. Kotov. *Modern Magnetooptics and Magnetooptical Materials*. 1997.

[21] V. Kletečka. Prostorově rozlišená měření Kerrova magnetooptického jevu v nanostrukturách. 2016.

[22] M. Faraday. Experimental researches in electricity.Nineteenth series. *Philosophical Transactions Royal Society*, 1845.

[23] J. Kerr. On rotation of the Plane of Polarization from the Pole of a Magnet. *Philosophical magazine and journal of science*, 1877.

[24] M. Nývlt. Optical interactions in ultrathin magnetic film structures. 1996.

[25] L. Beran. Studium fyzikálních vlastností heuslerových slitin. 2015.

[26] H. Fujiwara. *Spectroscopic Ellipsometry Principles and Applications*. Maruzen Co. Ltd, 2007.

[27] H. G. Tompkins. Spectroscopic Ellipsometry. https://www.aps.org/units/fiap/meetings/presentations/upload/tompkins.pdf. Accessed: 2020-10-05.

[28] E. Sebastian. *Lattice dynamics and spin-phonon coupling in the multiferroic oxides* $Eu_{(1-x)}HO_xMnO_3$ *and* $ACrO_2$. PhD thesis, 01 2019.

[29] A. S. Borovik-Romanov and H. Grimmer. International Tables for Crystallography. https://onlinelibrary.wiley.com/iucr/itc/Da/ch1o5v0001/sec1o5o1o2o2/. Accessed: 2020-14-05.

[30] D. Boldrin, I. Samathrakis, J. Zemen, A. Mihai, B. Zou, B. Esser, D. McComb, P. Petrov, H. Zhang, and L. Cohen. The anomalous Hall effect in non-collinear antiferromagnetic Mn_3NiN thin films. *Physical Review Materials*.

List of Figures

List of Tables

List of Abbreviations

AHE Anomalous Hall effect

DRAM Dynamic Random Access Memory

FCC field cooled cooling

FCW field cooled warming

IP in-plane

LSAT $(LaAlO_3)_{0.3}(Sr_2TaAlO_6)_{0.7}$

MOKE Magneto-optical Kerr effect

MRAM magnetic random access memory

OOP out-of-plane

p parallel

ROM Read Only Memory

s senkrecht, perpendicular

SRAM Static Random Access Memory

STO $SrTiO_3$

TE transverse-electric

TM transverse-magnetic

ZFC zero field cooling